Advancing alveolar in-vitro research with cell-line based air-liquid interface cultures

Master's Project in Molecular Biology, Molecular Genetics and Biotechnology
MOBN03 - 60Cr

Author

Setu Dambhare
Department of Biology, Lund University

Supervisor

Jenny Horndahl
Senior Scientist, Early Respiratory and Immunology, AstraZeneca
Linda Yrlid
Director, Early Respiratory and Immunology, AstraZeneca

Table of Contents

Abstract

Alveoli are sac-like structures in the distal lung specialised for gaseous exchange. Alveolar epithelium facilitates efficient respiration through a thin and robust arrangement of type-I (AT1) and type-II (AT2) pneumocytes, supported by tight junctions and surfactant-rich alveolar lining fluid. Chronic diseases like pulmonary fibrosis, asthma, and sarcoidosis compromise alveolar integrity, resulting in dysfunctions such as inflammation, edema, emphysema, or airway remodelling. In-vitro models are essential to understanding these molecular mechanisms in health and disease.

This study investigated the feasibility of four commonly used alveolar epithelial cell models in air-liquid interface (ALI) cultures. These included adenocarcinoma-derived A549 and H441 cells, and immortalised primary cell-lines Aelvi and Arlo. The models were evaluated for barrier formation, alongside phenotypic characterisation, and functional assessments. H441, Aelvi, and Arlo cells maintained a functional barrier for up to three weeks and expressed alveolar epithelium associated markers under ALI conditions. Despite transformation to serum-free media, A549 cells failed to develop a barrier and were not characterised further in this study.

Treatment with inflammatory and fibrotic stimuli reduced the transepithelial electrical resistance (TEER) and triggered release of interleukin-6 (IL6), Granulocyte-macrophage-colony stimulating factor (GM-CSF), interleukin-8 (IL8), and Chemokine (C-C motif) ligands - CCL5, CCL17, and CCL22, indicating onset of inflammatory response. Additionally, fibrotic treatment induced gene markers of aberrant basaloid differentiation as well as epithelial-mesenchymal transition, indicating potential to mimic fibrosis-driven tissue remodelling. The H441 model demonstrated AT2-like characteristics with surfactant expression and inflammatory responsiveness; Aelvi showed both AT1 and AT2 markers with pronounced fibrotic response; and Arlo cells developed a reactive TEER relevant for studying barrier function.

These findings demonstrate the strengths and limitations of different cell-line–based ALI models in studying alveolar biology. Further studies can explore their long-term stability and translational application. This would enable model matching to specific research needs, thus improving the relevance and impact of in-vitro ALI models in alveolar research.

Keywords - Alveolar epithelial cells, air-liquid interface culture, pulmonary surfactant, epithelial barrier function, transepithelial electrical resistance, model development, inflammatory cytokine response.

Abbreviations

AbBa cells – Aberrant Basaloid Cells

ABCA3 – ATP-binding cassette subfamily A member 3

AEC – Alveolar Epithelial Cells

ALF – Alveolar Lining Fluid

ALI – Air Liquid Interface

Alveolair (Epithelix$^{TM)}$ – A commercial ALI model of alveolar epithelium from company Epithelix with both AT1 and AT2 cells.

ARDS – acute respiratory distress syndrome

AT1 – Type 1 Pneumocytes

AT2 – Type 2 Pneumocytes

AQP1/2/3/4/5 – Aquaporin 1/2/3/4/5

BSA – Bovine Serum Albumin

CCL5/17/21 – Chemokine (C-C motif) ligand 5/17/21

CDH1 – E-cadherin

cDNA – Complementary deoxyribonucleic acid

COPD – Chronic Obstructive Pulmonary Disease

Ct – Cycle threshold

DAPI stain – 4\',6-diamidino-2-phenylindol stain

DMEM media - Dulbecco's Modified Eagle Medium

DMSO - Dimethyl sulfoxide

ECM – Extracellular Matrix

EMT – Epithelial Mesenchymal Transition

FC 1X/2X – Fibrotic Cocktail (Concentration 1X or 2X)

FN1 – Fibronectin

GM-CSF – Granulocyte-macrophage-colony stimulating factor

HBSS - Hanks' Balanced Salt Solution

Hi-FBS – Heat inactivated Foetal Bovine Serum

H&E stain – Haematoxylin and Eosin stain

IL 1β/6/8 – Interleukin 1-beta/6/8

IPF – Idiopathic Pulmonary Fibrosis

ITS – Insulin -Transferrin-Selenium

Krt17 – Keratin-17

LPA - Lysophosphatidic Acid

LPS – Lipopolysaccharide

MMP7 – Matrix Metalloproteinase 7

MSD assay – Meso Scale Discovery assay

PBS – Phosphate buffer saline

PCLS – Precision Cut Lung Slices

PDGF-AB – Platelet-Derived Growth Factor - AB

PDPN – Podoplanin

RNA – Ribonucleic acid

RPMI-1640 media – Roswell Park Memorial Institute-1640 media

RT-PCR – Reverse Transcription Polymerase Chain Reaction

TEER- Transepithelial electrical resistance

TGFβ – Transforming Growth Factor beta

TJP1 – Tight Junction Protein -1

TNFα – Tumour Necrosis Factor alpha

VIM - Vimentin

SAECs – Small Airway Epithelial Cells

SP-A/B/C/D – Surfactant Protein A/B/C/D

2D/3D cultures – Two dimensional/three-dimensional cultures

Introduction

Human airway – A complex system for gaseous exchange

The human respiratory system comprises multiple specialised compartments that form a complex network to facilitate gaseous exchange between the environment and the bloodstream. It can be broadly divided into two portions – the conducting part and the respiratory part. The former transports air from the environment to the respiratory portion, where the gaseous exchange takes place, resulting in oxygenation of the blood. The oxygenated blood is then transported throughout the body by the circulatory system. (Khan et al., 2024)

The conducting portion comprises the nose, nasopharynx, larynx, and trachea, leading to the pair of lungs. While structurally the left and the right lung are similar, their organisation differs. The lungs are compartmentalised into lobes. The left lung comprises two lobes and the right is divided into three. An arborescent arrangement of these specialised compartments leading to successive branches forms the 'tracheobronchial tree' (Figure 1). Residing within the lungs, the bronchi progressively branch into bronchioles. Primary bronchus constitutes the first order branch in each lung followed by the lobar bronchi. These are associated with the separate lobes. The final branches from the lobar bronchi are termed segmental bronchi, which are associated with the segments within each lobe. The bronchi lead to respiratory bronchioles. It is at this stage that we arrive at the respiratory portion of the human airway. The respiratory bronchioles further branch into the alveolar ducts which lead to the distal units of the respiratory system, the alveoli. These are small, monolayer, air-filled structures that serve as the primary site for gaseous exchange. Human lung contains approximately three to five hundred million alveoli providing nearly 70 – 140 square meters of surface area for gaseous exchange. (Ochs et al., 2004)

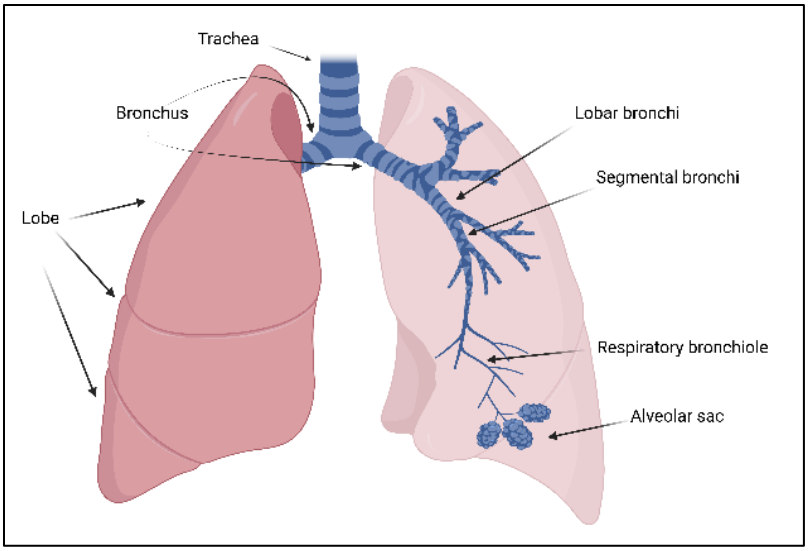

Figure 1. **Tracheobronchial tree**

Alveoli – the primary site for gaseous exchange

About 90% of the lung parenchyma is taken up by the alveolar region. Alveoli are arranged in functional clusters termed 'acinus.' Humans are estimated to possess around 15000 to 25,000 acini. Each acinus contains several alveoli with associated alveolar ducts branching out of the respiratory bronchioles (Reid et al., 2011; Weibel et al. 2005). Between the alveoli, reside the inter-alveolar septum which creates the structural landscape for gaseous exchange. A network

of blood capillary surrounds the alveoli. The alveolar wall and the surrounding capillary together form the air-blood barrier (Knudsen et al., 2018).

The conducting portion or the upper airway is responsible for filtering and warming up the incoming air. This ensures that the air is free from microbes and irritants and does not cause mechanical damage to the sensitive alveolar structure. This is achieved by a combined effort from a diverse population of specialized cells (Kia'i & Bajaj, 2019).

Alveoli, on the other hand, presents less constitutional diversity. The alveolar region mainly constitutes the alveolar epithelial cells (AECs) including type-I and type-II pneumocytes (AT1 and AT2 cells) and tissue resident alveolar macrophages (Figure 2). AT1 cells constitute up to 93%-95% of the alveolar surface. These squamous cells assume a thin organization to allow gaseous exchange. These cells are terminally differentiated and metabolically dormant. AT2 cells are cuboidal in structure and form 5%-7% of the alveolar surface. They are responsible for surfactant production and lowering the surface tension in the continuously expanding and collapsing alveoli during respiration. They possess specialized structures called lamellar bodies for production and storage of the surfactants. These cells are transcriptionally active and serve as pulmonary stem cells which can differentiate into AT1 cells on injury to maintain structural integrity (Brandt & Mandiga, 2023; Chuquimia et al., 2013).

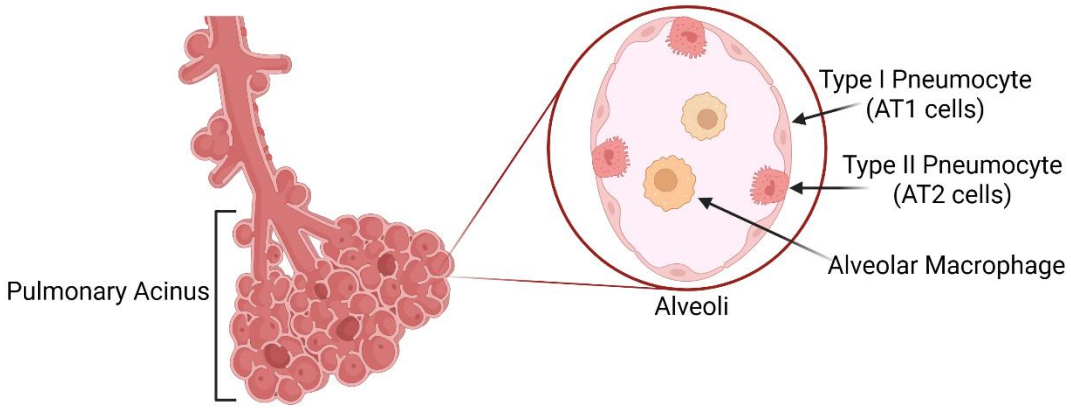

Figure 2. **Organisation of AT1 and AT2 cells in the alveoli**

Alveolar structure and function correlation:

The AT1 and AT2 cells form a simple and specialised monolayer for air exchange. However, the functional efficiency of the alveolar system is supported by various factors. To achieve gaseous exchange, a thin diffusion interface is important. In humans, the alveolar diffusion barrier is 1-2µm in thickness (Gehr et al., 1978). Furthermore, the alveoli are continuously subjected to volume changes. This raises the need for a robust structural organisation. Fibroblasts in the alveolar interstitium provide this support by secreting connective tissue fibres such as, collagen, fibronectin, and elastin that forms a rich extracellular matrix (ECM), ensuring alveolar plasticity (Chua et al., 2006). Conditions such as idiopathic pulmonary fibrosis (IPF) are associated with abnormal proliferation of fibroblasts which causes tissue stiffness leading to reduced lung flexibility (Ghonim et al., 2023).

While this combination of cellular compartments ensures flexibility and barrier thickness, a thin fluid layer covering the entire alveolar surface provides a protective interface to the epithelial monolayer (Figure 3). This alveolar lining fluid (ALF) reduces direct exposure to

incoming air, which may contain small particles and irritants (Martin, 2000). The oxygen entering the alveoli and the carbon dioxide leaving the capillaries diffuse through this fluid layer. Thus, the ALF provides a transition phase for the gases (Hollenhorst et al., 2011).

The ALF is mainly made up of water. The two hydrogen and one oxygen atoms in the water give polar properties to ALF. The oxygen atom in water attains a negative charge and the two hydrogen atoms form the positive fraction. Several such molecules create a combined force that pulls the water molecules close together. Due to the apical localisation of the ALF within the alveoli, this effect pulls the alveoli inwards, creating sufficient surface tension (Creuwels et al., 1997).

The radical traction from the ECM surrounding each alveolus neutralises some of this force by mechanically pulling the alveoli away from the centre (Knudsen et al., 2018). Within the alveoli, the surfactants from AT2 cells chemically reduce the surface tension. This ensures that the alveoli do not collapse during breathing (Whitsett et al., 2010).

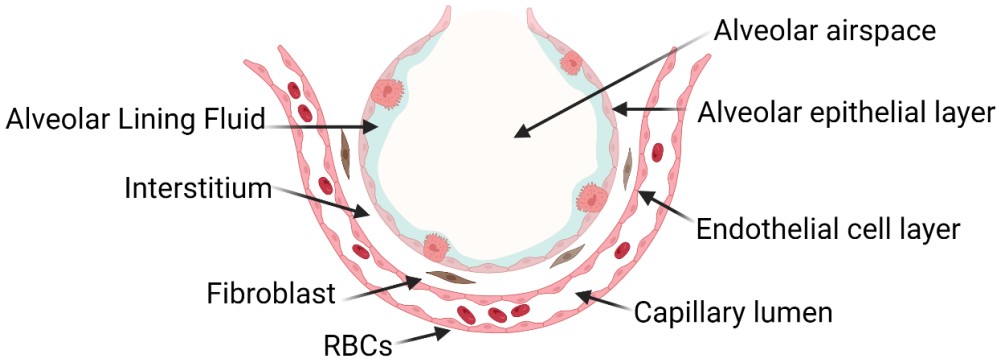

Figure 3. **Alveolar-capillary interface.**

Homeostasis and dysregulation

The limited cell diversity in the alveoli indicates that the AECs are capable of performing several functions to ensure homeostasis. For instance, these cells can secrete chemokines such as interleukin-8 (IL8) in response to injury or infection to recruit neutrophils and other specialised immune cells (Guillot et al., 2013).

AT1 cells possess several water and ion channels which ensure selective water transportation to always maintain the ALF layer and pressure, besides avoiding fluid build-up. Some characteristic markers include aquaporins (AQPs), podoplanin (PDPN) and sodium-potassium channels (Corrin et al., 2011). Furthermore, small flask shaped invaginations in the plasma membrane called caveolae (CAVs) provide mechanical stability during breathing and regulate inflammatory signalling (Kemp et al., 2008). AT1 cell growth is a major component in postnatal alveolar maturation and may influence neonatal lung disorders in pre-term birth (Yang et al., 2016). Furthermore, AT1 plasticity is an evolving frontier in studying remodelling linked to fibrosis and chronic obstructive pulmonary disorder (COPD) (Penkala et al., 2021; Aldahhan et al., 2025).

As described earlier, pulmonary surfactants are produced by the AT2 cells. Structurally these are 90% lipid (mainly phosphatidylcholine), 9% protein and 1% carbohydrate (Trapnell et al., 2003). There are four distinct apoproteins associated with the surfactant, namely surfactant

protein A, B, C, and D (SP-A/B/C/D). In addition to reducing the surface tension, as described earlier, the surfactants also play a vital role in inflammation. The lipid component can influence the cytotoxicity and lymphocyte proliferation, and the protein fraction guides specialised function. Hydrophilic protein SP-A and SP-D are associated with bacterial and viral clearance during infections (Han et al., 2015). Mutations in SP-A are linked to pulmonary fibrosis (Maitra et al., 2010).

Hydrophobic proteins SP-B and SP-C mainly regulate the physical environment in alveoli. SP-B influences lamellar body formation during early alveolar development along with lipid transporter proteins like ABCA3 (ATP-binding cassette, subfamily A, member 3). Mutations in either SP-B or ABCA3 are linked to respiratory distress syndrome and can have fatal outcomes in neonatal stages (Leibel et al, 2019; Shulenin et al., 2004). SP-C binds to lipopolysaccharides (LPS) on bacterial cell membranes mediating pathogen recognition (Augusto et al., 2002; 2003).

Finally, the AECs form tight junctions with adjacent cells to develop a strong and robust barrier. This ensures selective permeability to facilitate gaseous exchange while also monitoring the movement of molecules and pathogens across the epithelium (Herrero et al., 2015). The barrier integrity is specifically correlated with lung health. Conditions such as COPD, acute respiratory distress syndrome (ARDS), acute lung injury, emphysema, pulmonary fibrosis, chronic asthma, and some forms of cancer can damage the epithelial barrier (Kulkarni et al., 2016; Lucas et al., 2009). An impaired barrier results in increased permeability and poor fluid clearance, which lead to edema, as well as increased susceptibility to infections, toxins, and tissue damage. (Ware et al., 2001) Thus, the maintenance or disruption of the alveolar barrier is a critical factor in the pathogenesis and progression of several lung conditions.

Tools for Alveolar Research – Air-Liquid Interface Cultures.

The complexity of alveolar biology derives from the cross talk between different cell types and their microenvironment (Hogan et al., 2014). Hence, the alveolar function is affected by its structure and environment. Since these are the functional units for gaseous exchange, alveolar dysfunction causes severe lung diseases. While some conditions such as neonatal respiratory distress syndrome and bronchopulmonary dysplasia have developmental roots (Balest, 2023), other conditions like COPD, ARDS, and idiopathic pulmonary fibrosis (IPF) can be driven by tissue remodelling (Kulkarni et al., 2016; Lucas et al., 2009).

To properly understand the alveolar biology and dysfunction, it is important to understand the epithelial cell behaviour. However, the multicellular complexity and interdependency of AECs make their in-vitro modelling a challenging task. It is well documented that AECs fail to maintain their native phenotype in two-dimensional (2D) cell cultures and cannot create polarised cell layers. Moreover, they offer limited reproducibility due to donor dependent variations. (Kapalczynska et al., 2018).

Primary AT1 cells are fragile which makes them hard to isolate from the tissue. They may be prone to contamination with other cell types from the small airway (Evans et al., 2020). AT2 cells quickly change their phenotype to AT1 in-vitro and lose their proliferative capacity (Bears et al., 2017). To avoid this, AT2 cells can be grown in three-dimensional (3D) organoids or alveolospheres, however, the organoids are generally grown submerged in Matrigel or other

supporting matrices, and require a long generation time. The cells polarise towards the inside of the sphere which makes the apical surface inaccessible for direct manipulation and limits long-term experimentation (Vazquez-Armendariz et al., 2023). Although 3D cultures of primary AEC origin (such as Epithelix's AlveolAir co-culture or MetTek's Lung on Chip) are becoming available on the market, they offer limited scalability at a high cost. Furthermore, these commercial cultures are obtained fully matured and thus lack the ability for experimental customisation during differentiation. While these are shown to retain AT1 and AT2 cells as demonstrated by Lopes et al. (2025), they do not guarantee prevention of eventual phenotypic drift.

An advanced ex-vivo alternative for alveolar modelling is precision cut lung slices (PCLS). PCLS retain lung morphology with different cell types arranged in their natural orientation. However, this requires availability of tissue and is naturally associated with high costs and ethical considerations. Moreover, PCLS can also present donor dependent heterogeneity leading to difficulty in reproducing research findings. (Liu et al., 2022).

Both the alveolospheres and the PCLS model lack the critical component of transepithelial resistance (TEER), which is a widely used measure of barrier integrity. In addition, these systems have long generation times, high associated costs, limited accessibility for drug exposure, and structural limitations in exploring immune functions (Vazquez-Armendariz et al., 2023; Lieber et al., 1976). ALI cultures prove to be a viable alternative to resolve these limitations.

Air-liquid interface is an established cell culture technique where cells are cultivated on porous transwell membranes. The transwells orientation creates a basolateral and an apical chamber within the tissue culture plate wells. By removal of the apical media, air-exposure can be achieved promoting differentiation and polarised of the epithelial cell membrane. In context of AECs, the air exposure mimics the in-vivo lung physiology. Thus, promoting surfactant secretion by AT2 cells and enhancing tight junctions while supporting squamous AT1 like morphology (Abo et al., 2022). ALI also facilitate direct TEER measurement across the membrane (Jiang et al., 2018). This design allows access to both the upper and the lower surface of the cell layer for experimental manipulation. The apical surface can be easily treated with smoke, aerosols, pathogens, or drug candidates to study environmental factors, host-pathogen interactions, and drug absorption. Furthermore, by including fibroblasts, immune cells, or endothelial cells into the cultures, immune cell recruitment and cell-cell interactions can be explored. Given these practical considerations, Alveolar ALI cultures of different AEC cell-lines were applied in this study to evaluate their ability to replicate alveolar characteristics in-vitro.

Use of cell-lines for Alveolar ALI model

Immortalised cell-lines have long been used as accessible tools to study biological processes in-vitro. They present many advantages over primary cells, such as reduced cost, ease of cultivation, and long-term stability. They can be easily manipulated and generally produce reproducible findings in long term experiments.

A549 and H441 are two of the commonly used alveolar epithelial models of AT2 cells. A549 is a lung adenocarcinoma cell-line established in 1972 (Lieber et al., 1976). These cells maintain a basal epithelial morphology with multilamellar bodies and are highly referenced as

AT2 cells due to their partial surfactant production capacity (Korrodi-Gregorio et al., 2016). These cells, however, fail to develop a barrier in ALI, show a limited AEC expression profile (Ren et al., 2016), and their AT2 characteristics can be highly sensitive to cell culture conditions (Campiglio et al., 2021). Chary A., et al. in their 2022 paper, demonstrated an improved AEC phenotype in A549s grown in serum free media. In this project, A549 cells were transformed to serum free media conditions and assessed in ALI to check if the transformed cells (A549-T cells) could develop a functional barrier.

H441, on the other hand, shows a more specific AT2 profile with higher levels of all four surfactant proteins, SP-A, B, C and D as compared to A549 cells. In addition, H441s also produce other ion channel and transporter proteins such as, ATP binding cassette subfamily B member 1 (ABCB1) and solute carrier family 22 member 1 (SLC22A1) (Salomon et al., 2014). Established in 1982, this adenocarcinoma cell-line can produce tight junctions as well as a stable and functional TEER under ALI conditions (Lochbaum et al., 2020).

While cancerous cell-lines can produce reproducible and informative data, their altered genome and restricted expression profiles can be a limiting factor in adequately modelling alveolar physiology. In contrast, immortalised primary cell-lines have emerged as more physiologically relevant alternatives. Aelvi and Arlo are immortalised human alveolar epithelial cell-lines that have shown the capacity to form tight monolayers that recapitulate AT1/AT2 characters in vitro (Kuehn et al, 2016; Crius et al, 2023). Generated through lentivirus mediated immortalization, Aelvi cells present AT1 characteristics under submerged cultures, but show improved AT2 associated markers in ALI (Kuehn et al., 2016), indicating a mixed cell population. Arlo cells are the next generation cell line derived from Aelvi cells through single cell printing. With an improved and more uniform cell population, these cells can show an improved TEER and AT2 associated characters (Crius et al, 2023).

In this project, ALI models of the above-mentioned cell-lines were implemented and evaluated for their capacity to replicate the alveolar epithelium while avoiding the limitations and complexity of primary AECs, alveolosphere, and PCLS. The guiding hypothesis of this study was that immortalised alveolar epithelial cell lines can be cultivated in ALI to form a functional barrier which retains AEC characters, and responds to inflammatory and fibrotic stimuli to mimic the human alveolar barrier in-vitro. The barrier integrity was assessed through monitoring the TEER. Seeding densities were optimised and the gene expression profiles were checked for AT1/AT2 markers with RT-qPCR. The cell layer morphology was monitored through haematoxylin and eosin (H&E) staining of histology sections to check if the cells could form a thin monolayer similar to in-vivo samples. Junction and AT1/AT2 proteins were identified through confocal imaging and when possible immunofluorescent staining on histology sections. Once established, the cultures were stimulated with pro-inflammatory or fibrotic factors including, Tumour Necrosis Factor alpha (TNFα), interleukin-1 beta (IL1β), LPS, transforming Growth Factor beta (TGFβ) or fibrotic cocktail (FC) (Ptasinski et al., 2023) to evaluate the model's applicability in disease modelling. The effects of stimulations were analysed by monitoring TEER, induction of fibrotic markers, and secreted cytokines. Finally, epithelial cells were co-cultured with endothelial cells to investigate whether they influence the AEC expression profile as seen with primary cells. The different cell models were compared to identify a feasible in-vitro system which could mimic the alveolar epithelium for studying

biological function and disease pathogenesis, and potentially support early drug development and respiratory research.

Aims:

1. To establish and characterise ALI cultures of commonly used alveolar epithelial cell lines by comparing barrier formation, cell morphology and AEC associated gene and protein markers.
2. Functional assessment of the established ALI models in response to inflammatory and fibrotic triggers.
3. Determining the relative suitability of AEC models for applications in disease modelling and translational research.

Materials and Methods

Cell line expansion

All cell lines were expanded prior to experiments involving ALI. Aelvi (HuAelvi, Passage 11) and Arlo (HuArlo, Passage 11) cells were licensed from Inscreenex GmBh. H441 (Passage 54, ATCC) and A549 (Passage 7, ATCC) cells were obtained from AstraZeneca's internal cell bank. Aelvi, Arlo and H441 cells were expanded in cell culture flasks coated with AEC coating solution (Inscreenex, INS-SU-1018). A549 cells were grown in cell-bind tissue culture flasks (Corning, 3292).

Aelvi and Arlo cells were grown in huAEC basal media with huAEC Media supplements (Inscreenex, INS-ME-1013BS) according to the manufacturer's instructions (Inscreenex, 2025).

H441 and A549 cells were expanded in Roswell Park Memorial Institute-1640 medium (RPMI-1640, Gibco, A10491-01) and Dulbecco's Modified Eagle Medium (DMEM, Gibco, 31966-02) containing GlutaMAX, respectively supplemented with 10% heat inactivated fetal bovine serum (HiFBS, A5256801). The cells were seeded at the density of 2,67E+04 cells per cm2 and allowed to grow until 90% confluent. The cells were detached using TrypLE Select (Gibco, A12859-01) according to the product specifications (Thermo Fisher Scientific, 2024). Aelvi and Arlo cells were frozen using Inscreenex Freezing medium (INS-SU-1004) and the H441 and A549 cells were frozen with their respective media supplemented with 10% Dimethyl Sulfoxide (DMSO) and 20% HiFBS.

Air-Liquid Interface

The cells were seeded onto 24 well transwell plates (pore size 0.4µm, Corning # 3524) coated with AEC coating solution. Variable seeding densities were tested and 1,82E5 cells per cm^2 was picked for subsequent characterizations.

Aelvi and Arlo cells were grown in their routine AEC media for the entirety of the experiments. The cells were airlifted two to three days post seeding (on reaching nearly 100% confluence) and allowed to grow in ALI conditions. The basolateral media was changed every 2-3 days.

H441 cells were grown in RPMI-1640 supplemented with 10% Hi-FBS in submerged conditions. The media was changed every 2-3 days. Once nearly 100% confluent, the media was changed to differentiation media comprising basal media supplemented with 4% hi-FBS, 1% insulin-transferrin-selenium (ITS), and 1 µM dexamethasone.

A549 transformation to FBS free media conditions

To evaluate the barrier formation capacity of A549 cells in FBS free condition, the cells were transformed to CnT prime Airway epithelium media (CellNTech, CnT-PR-A). The cells were gradually transformed from DMEM containing FBS to CnT media over 6 passages with 20% decrease in FBS containing media every subsequent passage to get cells in 100% CnT media (A549-T cells) (Chary et.al, 2022). The cells were frozen in either media containing 10% FBS and 10% DMSO or CS10 (Costar # 210373) FBS free cell freezing media.

Untransformed A549 cells and transformed A549-T cells were seeded onto 24-well transwell plates (pore size 0.4µm) at a variable seeding density ranging from 3.03E4 to 1,21E5 cells per cm2. Cells were grown in submerged conditions until 100% confluent. Once confluent, the apical media was removed, and the basolateral media was replenished every 2-3 days.

Post-thaw cell proliferation measured by Incucyte

The post thaw cell viability was determined by loading approximately 100µl of cell suspension on the Nucleocounter NC100 cassettes for automated viability assessment. Viability was read using the Nucleocounter NC100 instrument (ChemoMetec). To check the post thaw proliferation of cells in different media conditions, the cells were seeded onto a 96-well plate in replicates of five with a seeding density of 30303 cells per cm^2. The cells were monitored for 5 days with phase contrast image acquisitions at 10X magnification every six hours using Incucyte SX5 (Sartorius). Confluence was calculated using Incucyte software's inbuilt basic analyzer for calculating % confluence.

TEER measurements

The transepithelial electrical resistance (TEER) was measured from the day of airlift using EVOM™ Manual Ohm Meter (World Precision Instruments, EVM-MT-03-01) (WPI, 2019).

The apical chamber was filled with 200µl 1X Hanks' Balanced Salt Solution (HBSS) containing magnesium and calcium ions, and the plates were allowed to cool down to room temperature (RT) for 15 to 20 minutes prior to TEER measurement.

The resistance was measured in Ohms and corrected to obtain the TEER values as follows:

$$TEER = (resistance_{sample} - resistance_{blank/control}) * Area\ of\ transwell$$

Blank = Resistance of well containing no cells or untreated cells.

Area of 24 well transwell insert = 0.33 cm^2

Histology sample processing – fixation, dehydration, paraffin embedding and sectioning

The transwells were fixed with 4% formaldehyde for 3 hours at room temperature. After washing, the membranes were cut out from the transwells and dehydrated using Magnus lean

high throughput tissue processor (Total Tissue Diagnostics) with ethanol dehydration program "1 mm biopsy with sponges". Dehydrated membranes were cut in half and embedded in paraffin.
4µm sample sections were prepared using Rotary Microtome HM355S (ThermoFisher Scientific). The slices were loaded onto charged adhesion glass slides (Superfrost Plus or TOMO) and allowed to dry overnight.

Haematoxylin and Eosin (H&E) staining

Autostainer ST5010 (Leica Biosystems) was used for deparaffinization and H&E staining protocol on the Superfrost Plus slides. The slides were preserved with pertex (Histolab #00840), and coverslips were mounted for long term storage. After overnight drying the slides were scanned using VS200 scanner (Olympus Life Science) and visualized using OlyVIA image viewer software.

Immunofluorescence staining of paraffin embedded samples

Sections mounted on TOMO high adhesion slides were baked at 60°C for one hour. The samples were deparaffinised by dipping the slides twice in Zylene for 5 minutes, followed by 2 times in 100% ethanol for two minutes, twice in 95% ethanol for 2 minutes, once in 70% ethanol for 1 minute and finally rinsing with double distilled water for 5 minutes at RT. Antigen retrieval was performed using KOS microwave histostation (Milestone^{TM} SRL) at 95°C for 15 minutes in 1X Diva Decloaker reagent (BioCare Medical).

Following the antigen retrieval, slides were permeabilized for 10 minutes with 0.25% Triton X100 and blocked with 3% Bovine Serum Albumin (BSA) in Phosphate Buffer Saline (PBS) for 1 hour. All the antibodies were diluted in the blocking buffer (3%BSA in PBS). The primary antibody incubation was carried out overnight at 4°C. Secondary antibody staining and nuclear staining with DAPI (4′,6-diamidino-2-phenylindole) were carried out for 45 minutes at RT in the dark. The stained slides were preserved with Prolong Gold (ThermoFisher Scientific, P36934) and stored at 4°C until scanning with Olympus VS200 scanner (Olympus Life Science) and visualized using OlyVIA image viewer software.

Table 1. **Antibody dilutions** used for IF staining on paraffin embedded histology sections.

Primary Antibody	**Host**	**Marker**	**Manufacturer**	**Dilution**
Anti – ABCA3 (PA5-52478)	Rabbit	AT2	Thermo Fisher	1:50
Anti – Surfactant Protein C (ABIN1388448)	Rabbit	AT2	Thermo Fisher	1:50
Anti – Surfactant Protein B (AB40876)	Rabbit	AT2	Abcam	1:50
Anti – HTII-280 (TB-27AHT2-280)	Mouse	AT2	Terrace Biotech	1:50
Anti – Aquaporin 5 (Ab92320)	Rabbit	AT1	Abcam	1:50
Anti – Podoplanin (NB11096423)	Mouse	AT1	Novus Biologicals	1:50
Anti E-cadherin (14472)	Mouse	Junction	Cell Signaling Technologies	1:50
Anti – Occludin (OC-3F10)	Mouse	Junction	Thermo Fisher	1:50
DAPI	-	Nuclear stain	Thermo Fisher	1:2000
Secondary Antibody			**Manufacturer**	**Dilution**
Anti Rabbit AlexaFluor 568			Thermo Fisher	1:100

Anti Mouse AlexaFluor 448	Thermo Fisher	1:100
Anti Mouse AlexaFluor 647	Thermo Fisher	1:100

Confocal Imaging

The transwells were fixed with 4% formaldehyde for 3 hours at room temperature followed by permeabilization with 0.25% Triton-X100 for 15 minutes at room temperature. The samples were blocked with Super Block (Thermo Fisher, 37580) for 1 hour at RT. The primary antibody incubation was carried out overnight at 4°C. Secondary antibody and nuclear staining with DAPI were carried out for 1 hour at room temperature in the dark. Both antibodies were diluted in antibody diluent S3022 from Agilent technologies according to table 2. The image analysis was performed in Signal Image Artist (SimA). The whole well mean fluorescent intensity was calculated for each antibody using SimA's inbuilt image analysis protocol. The mean values were adjusted for signal with the secondary antibody control and visualized using GraphPad PRISM.

Table 2. **Antibody dilutions** used for confocal imaging.

Primary Antibody	**Host**	**Marker**	**Manufacturer**	**Dilution**
Anti – ABCA3 (PA5-52478)	Rabbit	AT2	Thermo Fisher	1:200
Anti – Surfactant Protein C (ABIN1388448)	Rabbit	AT2	Thermo Fisher	1:100
Anti – Surfactant Protein B (AB40876)	Rabbit	AT2	Abcam	1:500
Anti – Aquaporin 5 (Ab92320)	Rabbit	AT1	Abcam	1:800
Anti – Podoplanin (NB11096423)	Mouse	AT1	Novus Biologicals	1:50
Anti E-cadherin (14472)	Mouse	Junction	Cell Signaling Technologies	1:100
Anti – Occludin (OC-3F10)	Mouse	Junction	Thermo Fisher	1:100
DAPI	-	Nuclear stain	Thermo Fisher	1:2000
Cell mask Deep red	-	Membrane	Thermo Fisher	1:10000
Secondary Antibody			**Manufacturer**	**Dilution**
Anti Rabbit AlexaFluor 568			Thermo Fisher	1:500
Anti Mouse AlexaFluor 448			Thermo Fisher	1:500
Anti Mouse AlexaFluor 647			Thermo Fisher	1:500

RNA isolation and Reverse Transcriptase (RT-PCR) to generate cDNA

The cells were lysed in RLT Plus cell lysis buffer (Qiagen) and RNA isolation was performed using Qiagen's protocol for 'RNeasy Plus 96 Kit' (Qiagen, RNeasy plus Kit, 2015). The ribonucleic acid (RNA) samples were collected in 50µl RNAse free water. RNA concentrations were detected using a Nanodrop Spectrophotometer (Thermo Scientific).

Complementary DNA (cDNA) synthesis was performed using the Applied Biosystems™ SimpliAmp™ Thermal Cycler and the High-Capacity cDNA Reverse Transcription Kit (Applied Biosystems, 4374966), according to kit instructions (High-Capacity cDNA Reverse Transcription Kit, 2024). Each reaction was carried out in the final volume of 40µl under the following conditions - 25°C for 10 minutes followed by 37°C for 2 hours, and 85°C for 5 minutes. The cDNA samples were stored at -20°C.

Taqman gene expression assay - qPCR for quantification of AT1/AT2 markers and Junction Proteins

cDNA was used as a template for qPCR with Taqman probes (Table 3). cDNA was diluted with nuclease free water to an appropriate volume according to the number of genes. A master mix was prepared for each gene containing 5 µl Taqman®Fast PCR MasterMix (4444557), 0.5 µl 20X FAM-tagged TaqMan™ Gene Expression Assay, and 1.5 µl nuclease-free water per reaction. The master mix volume was calculated according to the number of samples including extra 20% to account for volume reduction during pipetting. Each sample was run in triplicates with a reaction volume of 10 µl containing 3 µl cDNA and 7 µl of previously prepared PCR master mix. The final reaction was carried out in a 384 well plate. A no template control (NTC) and a reverse transcriptase negative (RT -) control were added for each gene. A commercial alveolar ALI culture, AlveolAir (Epithelix^{TM}) was used as the positive control. Alveolair is an established co-culture of primary alveolar epithelial and lung endothelial cells that sustains both AT1 and AT2 cells as well as barrier properties (Lopes et al., 2025). qPCR reaction was performed in the QuantStudio 7 Flex Real-Time PCR (qPCR) System with initial activation at 95ºC for 20 seconds followed by 40 cycles of 95ºC for 1 second and 60 ºC for 20 seconds. The graphs were evaluated, and cycle threshold (Ct) values were generated using QuantStudioTM Real-Time PCR Software version 1.3.

The values were normalised for the mean of three housekeeping genes, ActB, Hprt, and SDHA. The resulting values were adjusted against the expression levels of each gene in small airway epithelial cells (SAECs) to obtain fold change values. The calculations were performed as follows:

Ct_{mean} (house-keeping control) = ($Ct_{gene\ 1}$ + $Ct_{gene\ 2}$ + $Ct_{gene\ 3}$) / 3
Delta Ct (ΔCt) = $Ct_{sample} - Ct_{mean}$
ΔΔCt = $Ct_{Alveolar\ ALI\ sample} - Ct_{SAEC}$
Fold change = $2^{-\Delta\Delta Ct}$

Table 3. **List of TaqMan probes** (Thermo Fisher) to check AT1/AT2 cell associated markers.

Gene	Cell type - Function	Assay ID	Reference sequence	Amplicon size (bp)
SFTPA2	AT2 Surfactant	Hs06650175_g1	NM_001098668.3	71
SFTPB	AT2 Surfactant	Hs00167036_m1	NM_000542.3	100
ABCA3	AT2 Surfactant transport	HS00184543_M1	NM_001089.2	77
PDPN	AT1	hs00366766_m1	NM_001006624.1	58
CAV1	caveolar structure	HS00971716_M1	NM_001172895.1	66
AQP3	AT1 - water transport	hs00185020_m1	NM_001318144.1	63
AQP4	AT1 - water transport	hs00242342_m1	NM_001317384.1	92
TJP1	Tight junction	Hs01551871_m1	NM_001301025.1	63

CDH1	Tight junction	Hs01023895_m1	NM_001317184.1	80
Nkx21	Progenitor marker	Hs00968940_m1	NM_001079668.2	72
SCGB1A1	Club cells	Hs00171092_m1	NM_003357.4	69
SDHA	Housekeeping control	Hs07291714_mH	NM_001294332.1	64
Hprt1	Housekeeping control	Hs02800695_m1	NM_000194.2	82
ActB	Housekeeping control	Hs01060665_g1	NM_001101.3	63

Treatment with inflammatory and fibrotic stimulants

The three cell lines were seeded onto the transwells at the density of 1.82E5 cells per cm^2. The cells were allowed to develop a stable TEER for 10-12 days post airlift with media change every 2-3 days. When the TEER stabilised, the ALI cultures were stimulated basolaterally with the following five stimulants for 7 days in replicates of 3. The concentrations and expected responses are defined in table 4.

Table 4. **List of inflammatory and fibrotic treatments.** Components, concentrations, and function.

Stimulant	**Concentration**	**Function**	**Expected response**
E.coli derived Lipopolysaccharide	0.1 µg/ml or 10 µg/ml	Mimics bacterial infection	Induction of inflammation and secretion of cytokines.
Human TNFα	20ng/ml	Pro-inflammatory cytokine in infections and lung injury.	TEER reduction and release of inflammatory cytokines.
IL1β	10ng/ml	Mediates inflammation	Reduced TEER combined with cytokine and chemokine release.
TGFβ	10ng/ml	Master regulator of fibrosis	Compromised barrier integrity and induction of EMT and AbBa.
Fibrotic cocktail (Ptasinski et al., 2023)	1X or 2X	Mimics chronic fibrotic environment by a combination of pro-fibrotic factors.	Reduction in TEER and induction of fibrosis associated tissue remodeling through EMT and AbBa transitions.
Components in the Fibrotic cocktail. Concentrations of each component at 1X.			
Mouse TNFα			10ng/ml
Human TGFβ			5ng/ml
Platelet-Derived Growth Factor (PDGF-AB)			10ng/ml
Lysophosphatidic acid (LPA)			5µM

On day 7 of stimulation, basolateral media samples were collected for assessment of secretory chemokines and interleukins and stored at -80°C. Whole cell RNA lysates were collected, and gene expression of aberrant basaloid and fibrotic associated markers was checked with Reverse Transcription Quantitative Polymerase Chain Reaction (RT-qPCR) (Table 5).

Table 5. **List of Taqman probes** (Thermo Fisher) to check fibrotic markers in stimulated ALI cultures.

Gene	Cell type - Function	Assay ID	Reference sequence	Amplicon size (bp)
VIM	Mesenchymal cells - Filament protein	Hs00958111_m1	NM_003380.3	65
Krt17	Epithelial cells – Filament protein	Hs00356958_m1	NM_000422.2	82
MMP7	Epithelial cells and fibroblasts	Hs01042796_m1	NM_002423.4	64
FN1	Epithelial cells and fibroblasts	Hs01549976_m1	NM_001306129.1	81
CDH-1	Tight junction	Hs01023895_m1	NM_001317184.1	80

Quantification of secretory immune signalling molecules

Mesoscale Discovery (MSD) U-plex assay was used to detect and quantify pro-inflammatory immune signalling molecules in the basolateral media of stimulated ALI cultures from the different cell lines. The assay was performed in 96 well plate format, U-Plex® Biomarker Group 1 (human) Multiplex Assay (#K15067M-2). The MSD assay plate was prepared according to the manufacturer's instructions (*U-PLEX Custom Biomarker Group 1 (Human) Assays*, 2023). A separate plate was used for the detection of Interleukin 8 (IL8). The plates were coated with biotinylated capture antibodies linked to specific linkers. Calibrator standards and samples were diluted according to the manufacturer's instructions and 50µl of each was added to the plate and incubated for 2 hours at room temperature with shaking. For plates with the IL8 samples, the calibrator standard was diluted 1:2 to obtain the highest standard and thereafter a 5-fold serial dilution was performed over 7 steps to obtain a broader range of concentrations. The samples for IL8 estimation were diluted 50 times due to expected high levels. The standard curves were generated using Sigmoidal curve fit with a four-parameter logistic model (GraphPad Prism).

PBS with 0.05% Tween-20 (PBS-T) was used as the wash buffer. After washing, the samples were incubated for 1 hour with SULFO-TAG conjugated detection antibody at room temperature with shaking. The plate was washed thrice and read directly with MSD Gold Read buffer. The signal was detected using the MSD plate reader (software V 2.1.3).

Statistical analysis and data visualization

GraphPad Prism (Software Version 10, Dotmatics) was used to create standard curves and perform statistical analysis on datasets. A Sigmoidal curve fit with a four-parameter logistic model was used to generate the standard curves for MSD assay.

Unpaired t-test was used to check significance of change in junction protein expression between submerged and ALI cultures of each cell type on fold change data from Taqman RT-qPCR analysis. One way Analysis of Variance (ANOVA) was used to determine the significance of AT1 and AT2 marker expression compared to positive control using. All

statistical analyses were performed in GraphPad PRISM 10. When applicable, calculations were carried out in Excel (Microsoft). All graphs were generated using GraphPad PRISM 10.

ALI co-culture with endothelial cells

Alveolar epithelial cells (AECs) together with capillary endothelial cells form the air-blood barrier in-vivo. Their bidirectional signalling can improve the barrier function and phenotype retention of AECs in-vitro. To test this, three different endothelial cell lines namely, Hulec-5a, HUVEC and HpMEC were tested in co-culture with the three AEC cell lines. The endothelial cell lines were obtained from ATCC. The post thaw viability of the three cell lines was checked with a Nucleocounter NC100 instrument. All cells were more than 90% viable.

The transwell inserts were flipped over the reservoirs and coated with AEC coating solution. Under sterile conditions, the endothelial cells were seeded at a density of 1.52E5 cells per cm2 on the inverted transwell inserts in 50µl cell culture media. The cells were allowed to attach for 4-5 hours. The transwell inserts were inverted to the normal configuration, and the various AEC cell lines were seeded on the coated transwells at 1.82E5 cells per cm2. The cells were allowed to grow submerged in the epithelial cells' routine media. Once confluent, the cultures were airlifted. TEER was monitored for up to 3 weeks, and the cultures were harvested for qPCR analysis at the end.

Results

Cell line expansion and post thaw proliferation

Prior to air-liquid interface (ALI) culture, the cells were expanded and frozen in large batches to ensure consistent cell availability and uniform passage throughout the experiments. Aelvi, Arlo, and H441 cells were expanded in their respective media. A549 cells were expanded in DMEM media containing 10% HiFBS. A batch of A549 cells was transformed to serum-free CnT Prime Airway media (A549-T) to test if the cells grown in FBS free conditions showed improved junction formation under ALI conditions. No antibiotics were used in any of the culture media to avoid interference with mitochondrial function, protein synthesis or stress responses. The presence of antibiotics can ultimately lead to selection of resistant cell colonies and reduce the physiological relevance of the models in later stages.

During expansion, it was observed that the Aelvi and Arlo cells grew rapidly and formed a continuous cell layer. H441, on the other hand, grew slowly and formed several individual colonies throughout the plate bottom, which eventually connected to form a continuous cell layer (Figure 4).

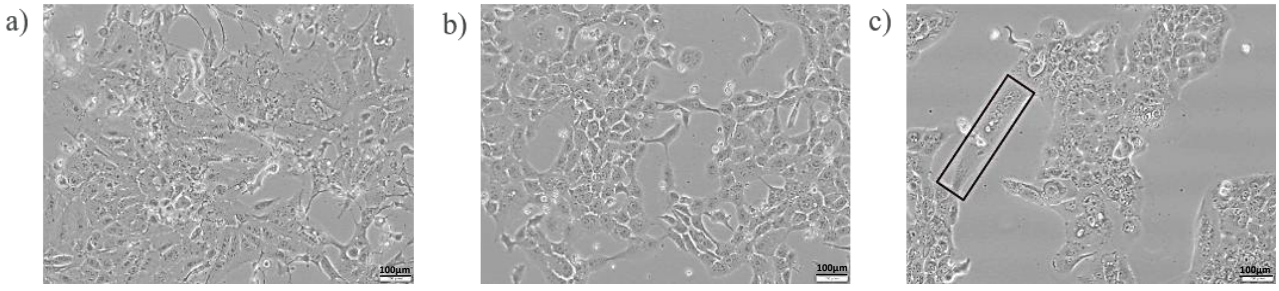

Figure 4. **AEC cell lines in submerged cultures**. Phase contrast images (10X magnification, scale 100 µm). Cells expanded in tissue AEC coating solution treated tissue culture flasks. a) Aelvi b) Arlo and c) H441 cells – box showing individual H441 colonies connecting via elongated cells.

A549 cells showed faster proliferation with sequential adaptation to CnT media. The cell morphology changed on transformation. A549-T cells had enlarged cells with prominent junctions, as compared to normal A549s after the same number of passages (Figure 5).

a) b)

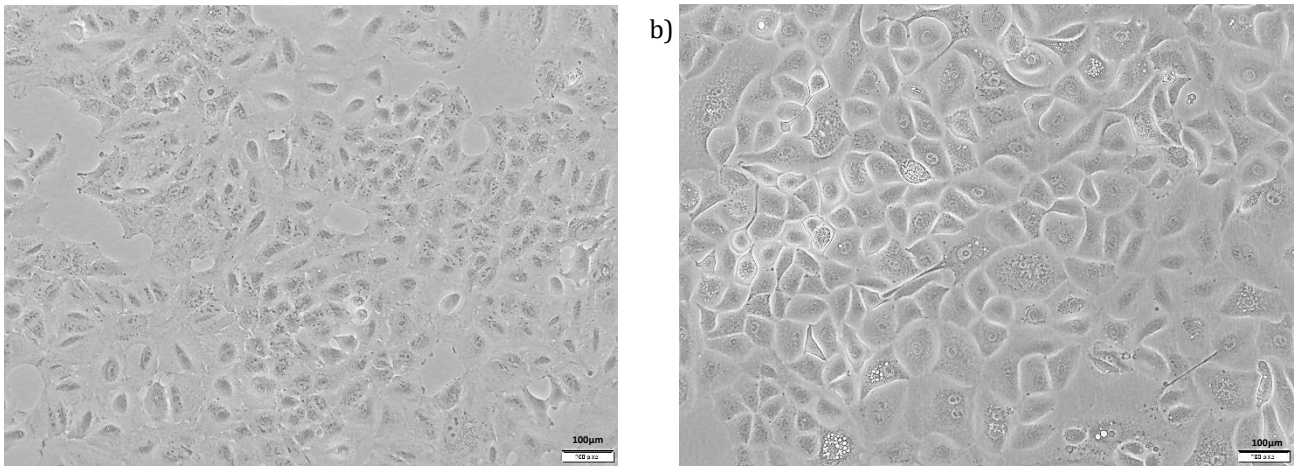

Figure 5. **Phase contrast images of A549 cells in different media conditions.** Cell grown in cell culture treated cellBIND flasks (Corning), maintained over five subsequent passages. Scale - 100µm, magnification - 10X. a) A549 cells grown in DMEM media supplemented with 10% Hi-FBS. b) A549-T cells transformed to serum-free CnT Prime Airway media.

The quality of frozen batches was determined by checking the post-thaw viability and cell proliferation. The post-thaw viability was evaluated with Nucleocounter NC100 instrument's automated viability assessment. All cell lines were more than 85% viable immediately post-thaw (Fig. 6a).

Cell proliferation was evaluated by monitoring cell growth for 5 days using phase contrast image analysis on the Incucyte SX5 system. Aelvi and Arlo cells reached maximum confluence in 2-3 days. H441 showed slow proliferation and reached approximately 70% confluence by day 5. A549 cells grown in DMEM media supplemented with Hi-FBS proliferated quickly and reached approximately 90% confluence by day five. A549-T cells showed negligible proliferation over five days, regardless of the freezing medium used. Growth remained stagnant after medium was changed, indicating low proliferative capacity following the freeze-thaw cycle (Fig. 6b).

a) b)

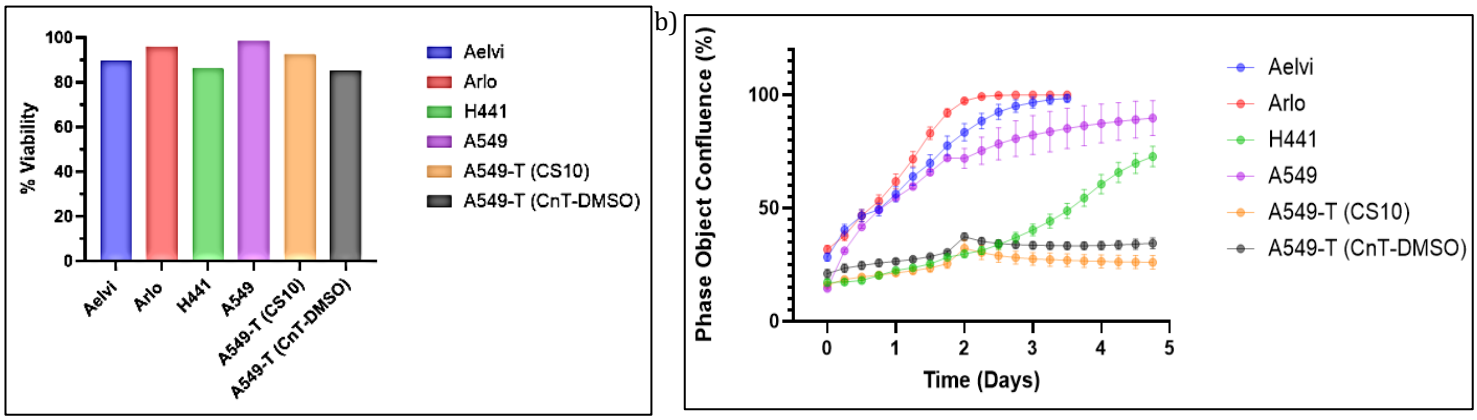

Figure 6. **Post-thaw cell viability and proliferation of AEC cell lines following expansion and freezing.** a) Percentage viable cells directly after thawing calculated with Nucleocounter NC100. b) Post-thaw cell proliferation observed over five days via whole well phase contrast imaging analysis using Incucyte SX5

instrument. All cells seeded on a 96 well plate in replicates of 5 at a density of 30303 cells per cm^2. Phase object confluence (%) determined by incucyte software (v2020C) – basic confluence analyser. Each data point representing mean with standard variations.

A549 cells lack barrier formation capacity in air-liquid interfaces.

Alveolar epithelial cells generally form a robust barrier in-vivo to facilitate air exchange and selective permeability of molecules. The barrier integrity is thus one of the major characteristics of alveolar biology. To evaluate the different cell lines for their barrier formation capacity, each cell line was grown on ALI transwells and the transepithelial electrical resistance (TEER) was measured over 2 weeks. For the A549 cells, while cell proliferation could be noted, no TEER was recorded with either non-transformed A549s or the A549-T cells. The latter formed an irregular cell layer (Fig. 7). Due to no recorded TEER, A549 cells were excluded from further characterisations in this project.

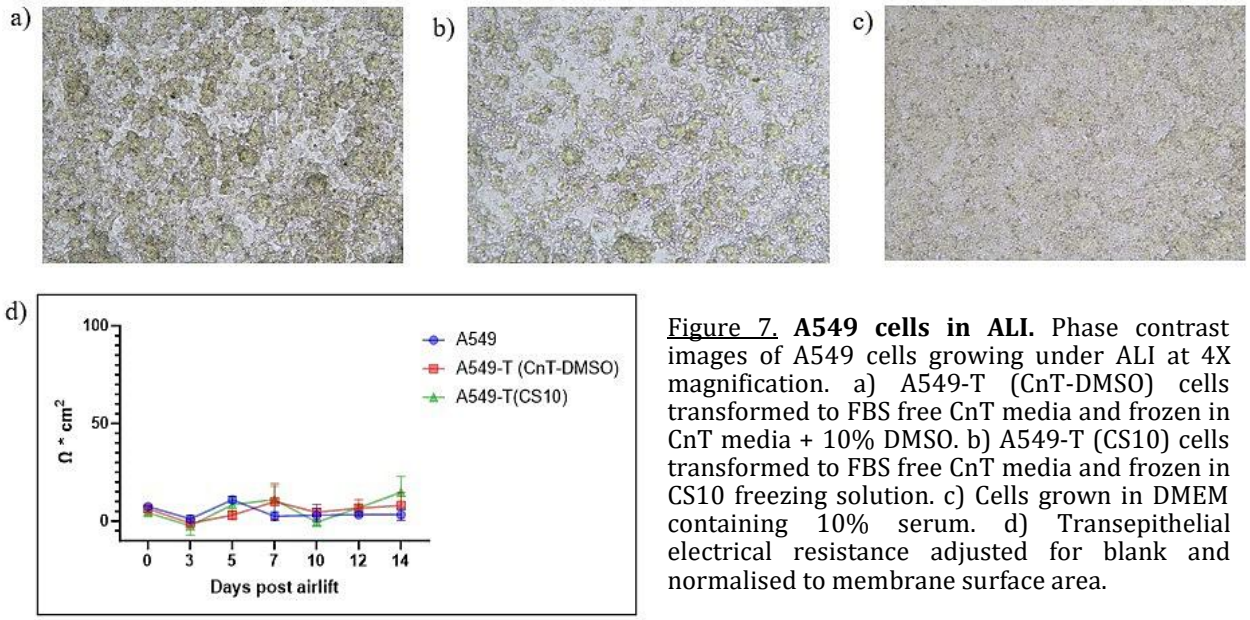

Figure 7. **A549 cells in ALI.** Phase contrast images of A549 cells growing under ALI at 4X magnification. a) A549-T (CnT-DMSO) cells transformed to FBS free CnT media and frozen in CnT media + 10% DMSO. b) A549-T (CS10) cells transformed to FBS free CnT media and frozen in CS10 freezing solution. c) Cells grown in DMEM containing 10% serum. d) Transepithelial electrical resistance adjusted for blank and normalised to membrane surface area.

Optimising seeding density

Aelvi, Arlo and H441 cells showed TEER formation in ALI. The manufacturer's protocol for Aelvi and Arlo cells recommended a seeding density of 3,03E5 cells per cm^2. Publications for H441 cells recommend seeding densities ranging between 3.03E4 and 1.21E5 cells per cm^2.

To standardise the comparison of the three cell lines further on, different seeding densities were tested in ALI. The cells were allowed to get 100% confluent in submerged condition. Once confluent, the apical media was removed, and the cells were allowed to differentiate and develop a TEER with air-exposure. The average TEER values presented here were calculated from an independent experiment with 24 replicate wells for each cell type. Aelvi and Arlo cells showed fast proliferation and were ready for airlift after 1-2 days in culture. The TEER normalised irrespective of the seeding densities after 1 week in ALI to reach 2150 ± 145 $\Omega.cm^2$ for Aelvi and 896 ± 160 $\Omega.cm^2$ for Arlo cells. H441 cells grew slowly. With lower seeding densities, the cells needed up to one week to reach >90% confluence. The TEER showed a

seeding density dependent trend initially and normalised to the same levels around day 10 to reach 250 ± 30 Ω.cm^2.

At 1,82E5 cells per cm^2, H441 cells grew quickly and were ready to air-lift at nearly the same time as the other two cell lines. This was picked as the appropriate seeding density for the experiments further on for all three cell types (Figure 8).

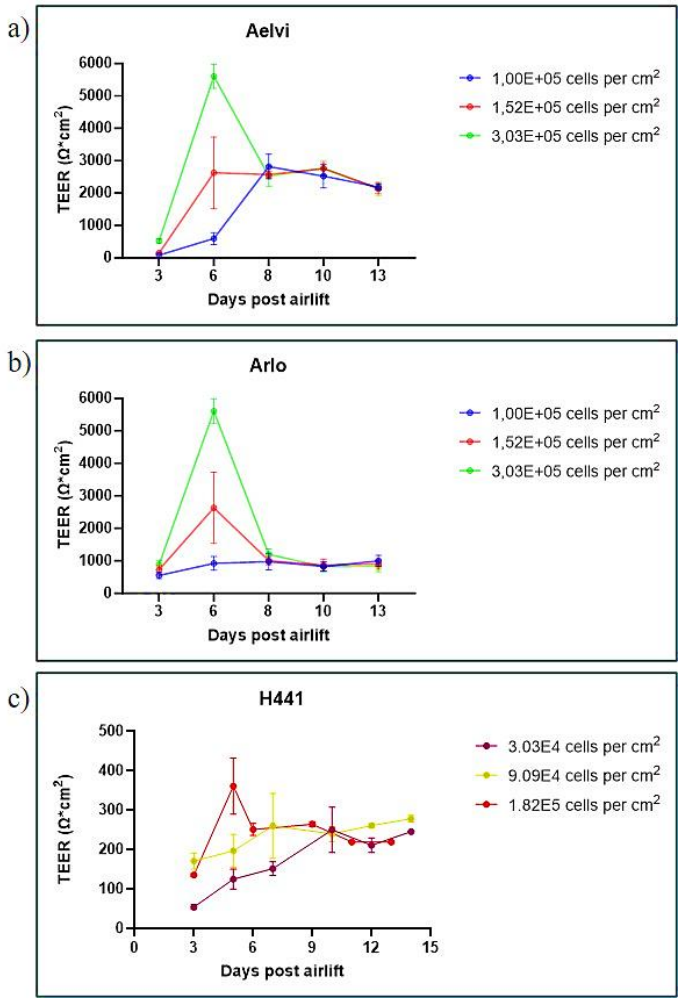

Figure 8. **Effect of seeding density on the transepithelial electrical resistance (TEER) of different alveolar epithelial cell lines cultured in air-liquid interface.** Post thaw TEER monitored over two weeks during each media change with EVOM™ Manual Ohm Meter (World Precision Instruments). Raw ohm measurements corrected for membrane resistance from an empty well without cells and adjusted to membrane surface area. Data from independent experiment with multiple replicate wells. a) Aelvi and b) Arlo cells (n=5). c) H441 (n=3).

Air exposure is important for barrier development.

To evaluate the role of air exposure in alveolar epithelial barrier development, paraffin embedded membrane sections were stained with haematoxylin and eosin (H&E stain) to visualise the cell layer morphology.

From histology sections on day 18 of the culture, it is clear that Aelvi and Arlo cells organise in a thin layer in both ALI and submerged conditions. However, clear gaps could be seen between the cells in submerged conditions indicating poor junction formation. H441 cells formed a thick cell layer in ALI with large vacuoles. However, the cell layer looked compact with few breaks. Submerged H441 culture formed a thinner cell layer which is ideal for alveolar modelling, but had several breaks in the layer indicating low tight junction formation (Figure 9).

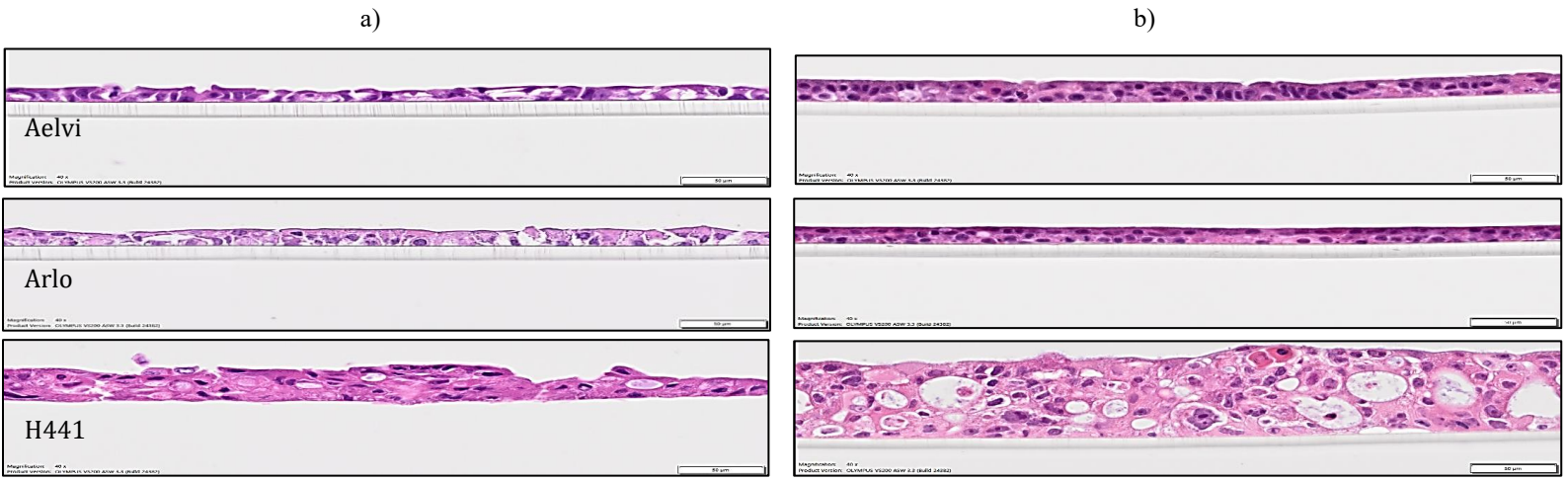

Figure 9. **Paraffin embedded histology sections stained with haematoxylin and eosin (H&E stain)**. 4µm thick histology sections showing cell layers with nuclei (blue) and cytoplasm (pink) from a) submerged or b) ALI cultures of Aelvi, Arlo or H441 cells scanned through Olympus VS200 at 40X magnification; scale bars – 50 µm

The epithelial barrier integrity was further confirmed by monitoring TEER development in submerged versus ALI cultures for each cell line. Aelvi and Arlo cells initially developed a higher TEER in submerged culture as compared to ALI. Eventually, a drop in TEER was noted in submerged cultures while the TEER continued to grow under ALI conditions. H441 showed improved TEER with ALI throughout the experiment (Figure 10).

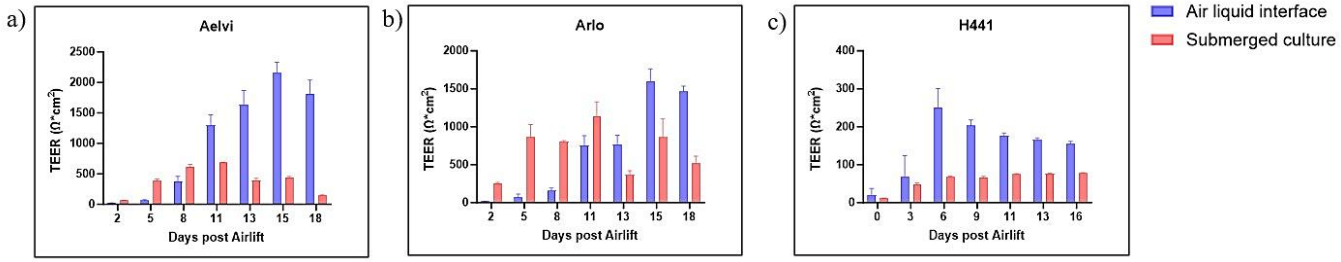

Figure 10. **Trans-epithelial electrical resistance between submerged (no of wells =2) and air-liquid interface (ALI) cultures (no of wells =3).** a) Aelvi, b) Arlo and, c) H441 cells cultured in submerged and ALI condition. TEER monitored for 16 to 18 days post airlift during every media change. Raw ohm measurements adjusted for membrane resistance from an empty well and normalised to membrane surface area. Bars representing mean with standard error.

Finally, the gene expression of E-cadherin (CDH1) and tight junction protein (TJP1) was compared between submerged and ALI cultures with TaqMan gene expression assay. Consistent with TEER and histology observations, a significant increase in junction proteins was observed for all cell types with an exception of CDH1 in Aelvi cells (Figure 11). These

observations together confirmed that air-exposure significantly improves the barrier formation of alveolar epithelial cell lines, justifying the need for ALI cultures.

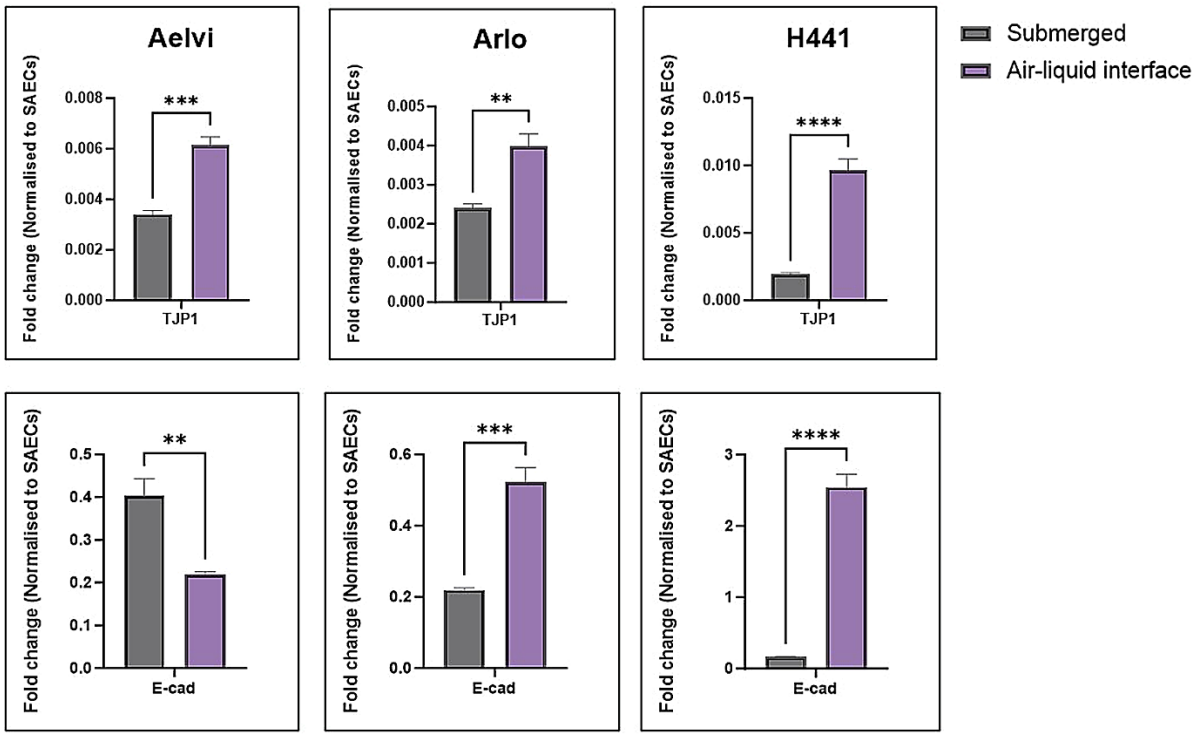

Figure 11. **Junction proteins in Submerged versus air-liquid interface (ALI) cultures (n=3).** Fold change (2^ΔΔCT) mRNA levels of tight junction protein (TJP1) and E-cadherin (CDH1) assessed using Taqman RT-qPCR assay normalised to expression in primary small airway epithelial cells. Aelvi and Arlo samples collected on day 18 post airlift, H441 samples collected 16 days post airlift. Statistical significance determined using unpaired two-tailed t-test $p < 0.05$ (*), $p < 0.01$ (**), $p < 0.001$ (***), $p < 0.0001$ (****).

Characterising AT1/AT2 markers

After confirming barrier formation in the three cell lines, the cell identity was evaluated by looking at the gene expression of type-1 and type-2 cell (AT1 and AT2 cell) associated markers. Change in expression level was determined with the help of TaqMan gene expression assays. The expression levels were adjusted for housekeeping genes, SDHA, Hprt1 and ActB. The fold change was calculated against relative expression of the markers in small airway epithelial cells (SAECs) grown in ALI. This was the best available control for normalising the three cell lines for comparison with each other in the given experimental set up. A threshold cutoff was set at cycle threshold (Ct) value of 30 with exception for surfactant protein B gene (SFTPB), where SAECs had a Ct value of 34 but this protein was included in the analysis due to high expression in H441. Cell lysates from a commercial primary cell based alveolar ALI model - Alveolair (Epithelix ^{TM}) was used as a positive control. This commercial model is grown in ALI condition and claims to contains both primary AT1 and AT2 cells, as well as fibroblasts. Thus, this served as a very close physiological system to the models which were evaluated in this study.

H441 showed high gene levels of surfactant genes - SFTPA, SFTPB, and ABCA3, consistent with the AT2 identity of the cell line. The expression levels were many folds higher than the positive control. Aelvi and Arlo showed higher levels of ABCA3 than the positive control but negligible surfactant production (Figure 12).

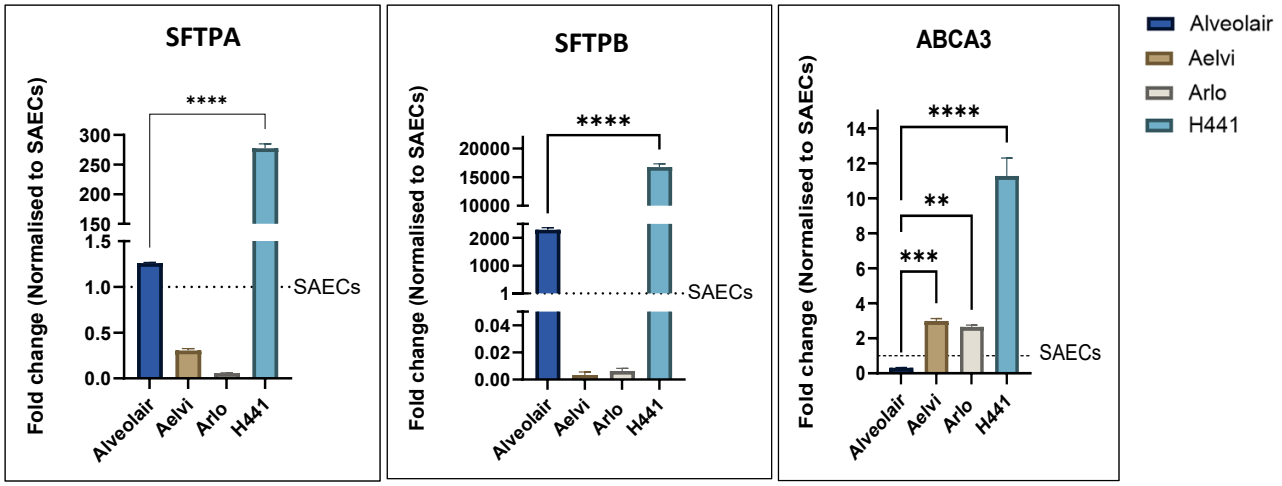

Figure 12. **Type-2 (AT2) associated marker expression.** Relative expression of AT2 markers represented as fold change (2^ΔΔCT) normalised to expression levels in small airway epithelial cells compared with positive control 'Alveolair' commercial ALI system. Aelvi and Arlo samples collected on day 18 post airlift, H441 samples collected 16 days post airlift. Statistical significance evaluated by one way ANOVA $p > 0.05$ (ns), $p < 0.01$ (**), $p < 0.001$ (***), $p < 0.0001$ (****).

H441 showed a high aquaporin 4 (AQP4) and low caveolin 1 (CAV1) gene expression. Aelvi and Arlo cells expressed CAV1 and Aquaporin 3 (AQP3). However, the expression was significantly lower than the positive control. Arlo showed higher expression of CAV1 and Aelvi showed more AQP3 production (Figure 13) suggesting functional differences in these two cell lines.

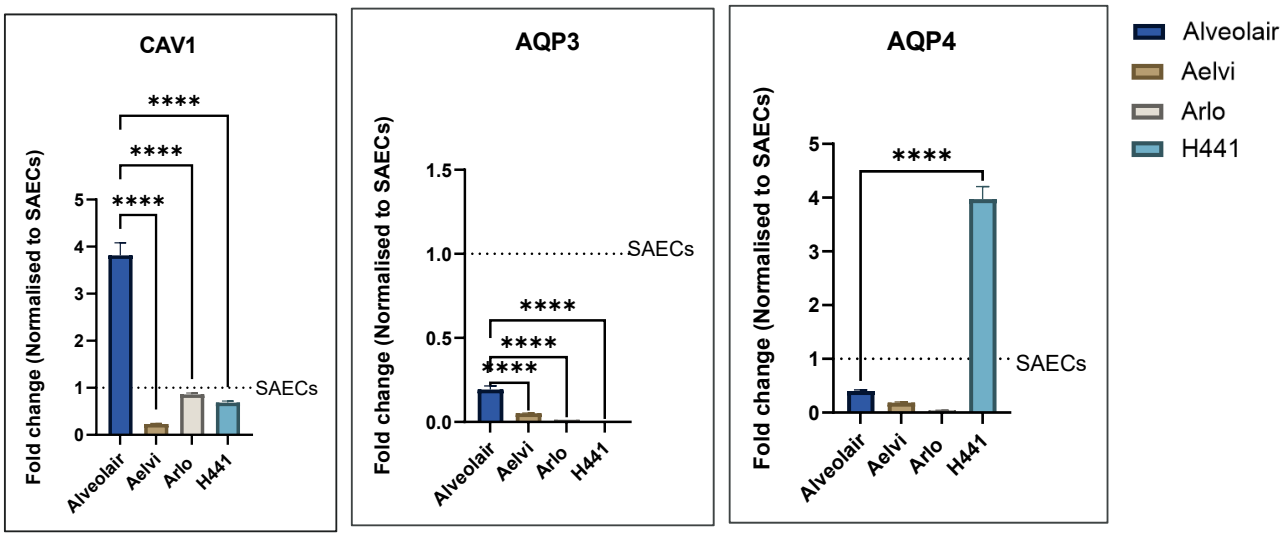

Figure 13. **Type-1 (AT1) associated marker expression.** Relative expression of AT1 markers represented as fold change (2^ΔΔCT) normalised to expression levels in small airway epithelial cells compared with positive control 'Alveolair' commercial ALI system. Aelvi and Arlo samples collected on day 18 post airlift, H441 samples collected 16 days post airlift. Statistical significance evaluated by one way ANOVA $p > 0.05$ (ns), $p < 0.01$ (**), $p < 0.001$ (***), $p < 0.0001$ (****).

All three cell models exhibited both AT1-associated and some AT2-associated markers at the gene level, indicating a mixed cell population within the ALI cultures.

While many AT1 and AT2 gene markers could be detected with qPCR, some of the most common markers, such as, surfactant protein C (SP-C), aquaporin 5 (AQP5), and podoplanin

(PDPN), were expressed at a low level or not detected at all (data not shown). To check the expression of these markers at the protein level, confocal imaging assay was performed on fixed and permeabilised ALI inserts stained with specific antibodies. Additionally, immunofluorescence staining was carried out on paraffin embedded sections. The transwells were imaged using Yokogawa CV8000 confocal microscope. The sections were scanned with Olympus VS200 scanner.

AT2 markers SP-B, SP-C and ABCA3 were detected with confocal imaging assay and quantified as the whole well mean fluorescent intensity for each secondary antibody (Figure14). SP-C, which was not detected with qPCR, was detected with imaging for all three cell lines.

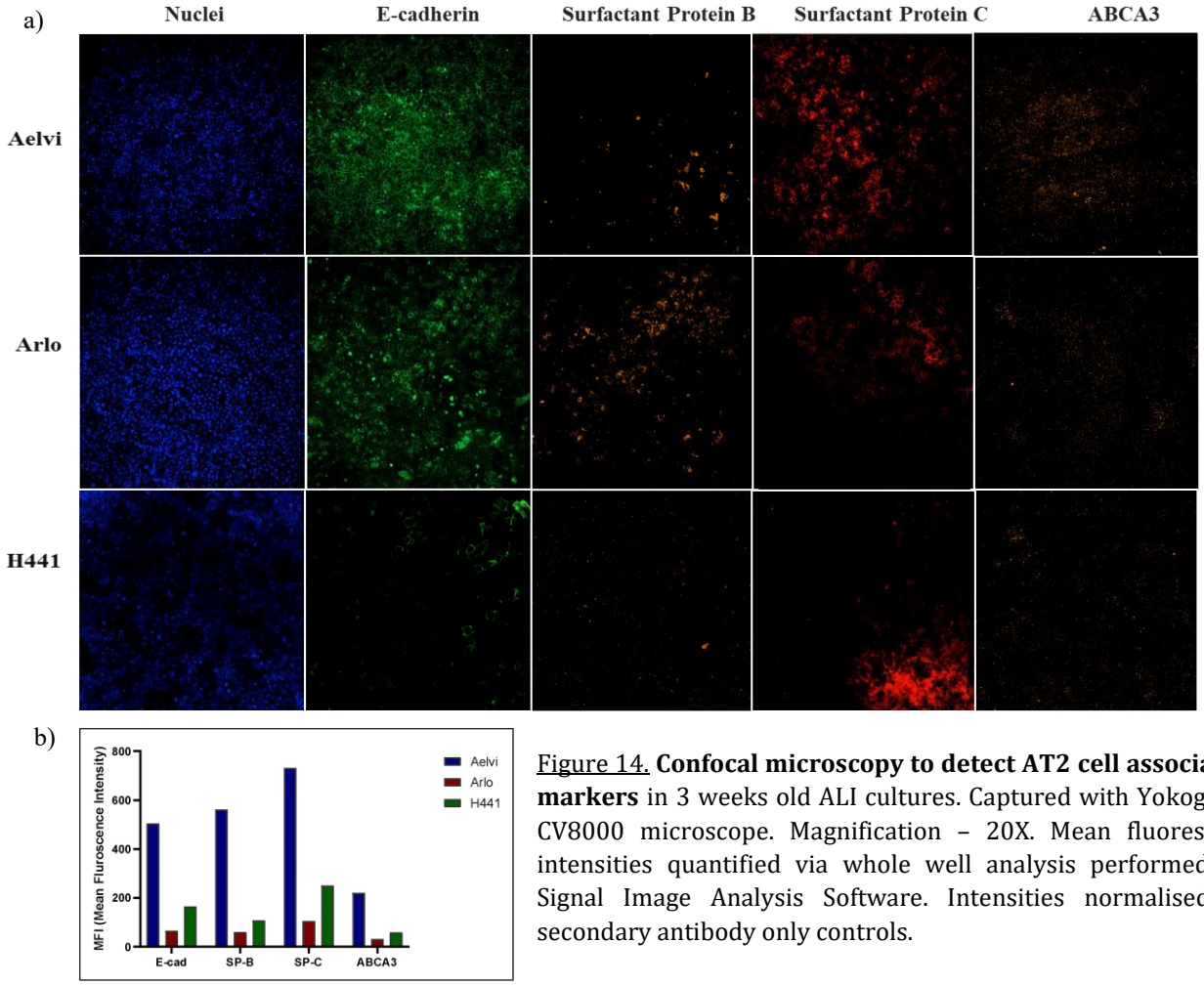

Figure 14. **Confocal microscopy to detect AT2 cell associated markers** in 3 weeks old ALI cultures. Captured with Yokogawa CV8000 microscope. Magnification – 20X. Mean fluorescent intensities quantified via whole well analysis performed on Signal Image Analysis Software. Intensities normalised to secondary antibody only controls.

Similarly, AT1 markers, AQP5 and PDPN were detected with confocal imaging. Aelvi expressed both PDPN and AQP5. Some PDPN could be detected in Arlo but H441 showed nearly no signal for either of the two markers (Fig 15).

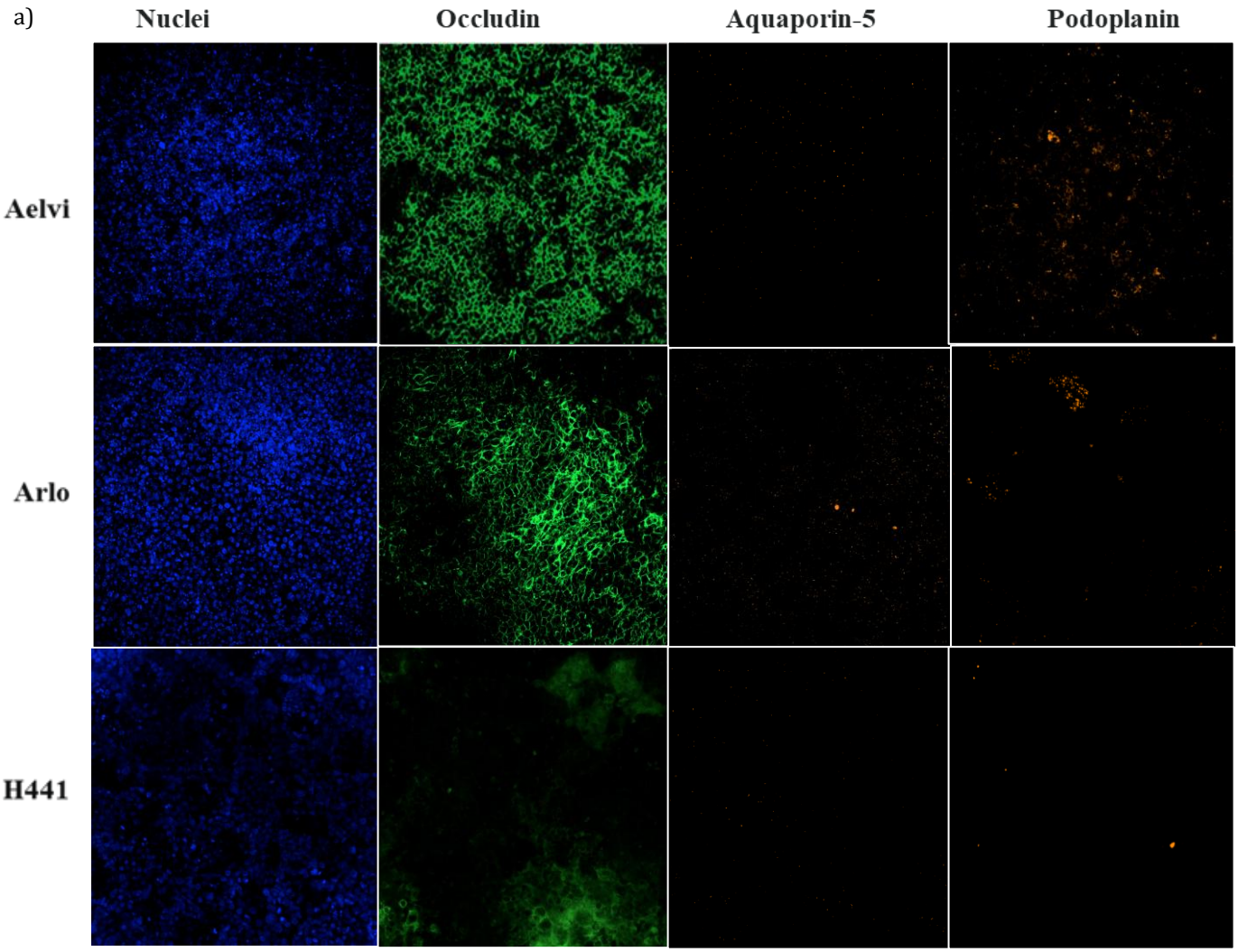

b)

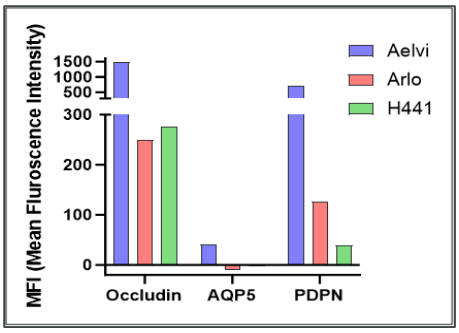

Figure 15. **Confocal microscopy to detect AT2 cell associated markers** in 3 weeks old ALI cultures. Captured with Yokogawa CV8000 microscope. Magnification – 20X. Mean fluorescent intensities quantified via whole well analysis performed on Signal Image Analysis Software. Intensities normalised to secondary antibody only controls.

IF staining on histology sections was used to look at localisation of different proteins in the cell layer. The staining protocol was performed manually. H441 showed AT2 markers, Surfactant protein C (Figure 16a), Surfactant protein B (Figure 16b) and HTII-280 (Figure 16c). HTII-280, which is a AT2 specific marker used for isolating AT2 cells from lung tissue (Gonzalez et al., 2010), was also seen localised within the Arlo cell layer but was not detected in Aelvi cells (Figure 16c). Aelvi and Arlo sections formed thin cell layers. As a result, they could not withstand the manual staining protocol in most cases due to the thin cell layer getting disrupted. No AT1 markers could be detected in either of the cell lines.

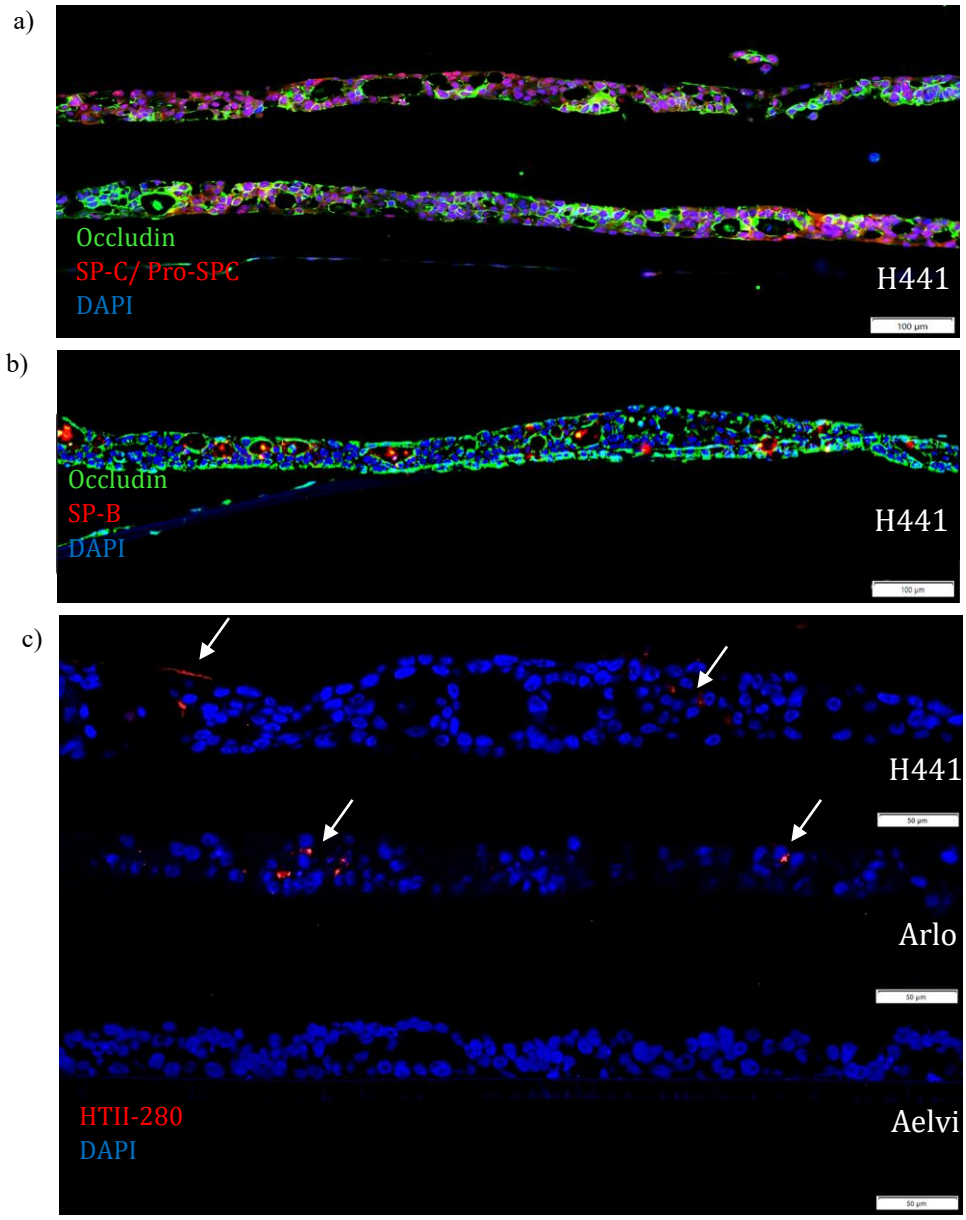

Figure 16. **Immunofluorescent staining on paraffin embedded histology sections against AT2 cell associated markers.** H441, Aelvi and Arlo sectioned fixed and stained for junction protein Occludin and AT2 markers (surfactant proteins - SP-C, SP-B and HTII-280). Nuclei counterstained with DAPI. Image acquisition using Olympus VS200 Scanner at 40X magnification. a) Scale 100µm; Pro-SPC and SP-C concentrated within H441 cell layer. b) Scale 100µm; SPB localised within empty air-filled vacuoles in H441 cell layer. Appearance of vacuoles containing SPB. c) Scale 50µm; HTII-280 in H441 and Arlo cells.

Functional assessment:

After confirming the presence of the various AEC markers in the ALI cultures, the models were tested for their functionality. The cell lines were grown in ALI and allowed to develop a TEER according to the set protocol. Once the TEER stabilised, the cells were treated with pro-inflammatory stimulants for one week. The treatments included tumour necrosis factor alpha (TNFα), interleukin-1 beta (IL1β), E.coli lipopolysaccharide (LPS), transforming growth factor beta (TGFβ) or fibrotic cocktail (FC). The effect of the stimulants on TEER was monitored throughout the stimulation time-period. LPS treatment did not show any significant effect on

the TEER for any of the cell lines. Aelvi cells showed a drop in TEER in response to the FC and TGFβ. H441 cells showed delayed TEER drop starting 4th day onwards with FC and TNFα treatment. Arlo cells were sensitive and exhibited a significant drop in TEER in response to each treatment except LPS (Figure 17).

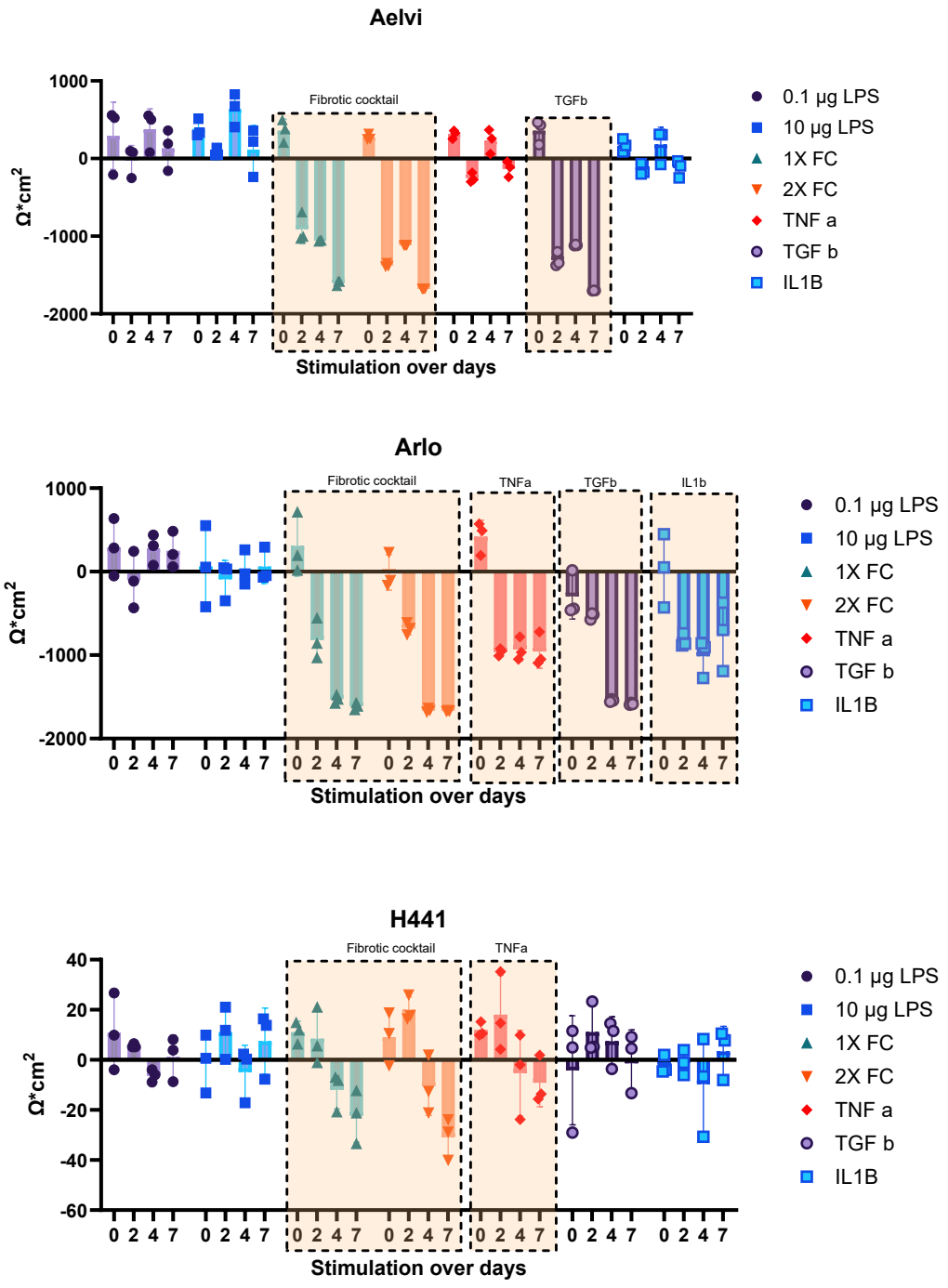

Figure 17. **Effect of inflammatory and fibrotic stimulants on the transepithelial electric resistance (TEER).** The TEER was monitored during treatment with LPS (0.1 and 10 µg/ml), Fibrotic cocktail (1X and 2X), TNFα (20ng/ml), TGFβ (10ng/ml), and IL1β (10ng/ml) over 7 days. TEER measurements carried out during each media change. Raw ohm measurements normalised against non-treated control for each day and adjusted for membrane surface area. The three cell lines have different average TEER; thus, the Y axis represent different ranges specific for each cell line.

Production of pro-inflammatory cytokines and chemokines in response to stimuli.

Epithelial cells can induce immune response by secreting cytokines to indicate inflammation and cellular damage. To check whether the cell-lines in ALI cultures could recapitulate the secretory function of AECs on exposure to pathological triggers, an MSD panel was used to detect the presence of interleukins and chemokines in the basolateral media of the different ALI cultures after 7-days of treatment with inflammatory and fibrotic stimuli.

While no cell line lost barrier integrity in response to LPS treatment, Aelvi cells showed increased interleukin8 (IL8), and C-C motif chemokine ligands CCL17, and CCL22. At high concentration of LPS (10ug/ml), Arlo produced low levels of IL8, CCL5, and CCL17 (Figure 18). H441 did not produce any interleukins in response to LPS but had a slightly increased level of granulocyte-macrophage colony-stimulating factor (GM-CSF). Additionally, CCL5/17/22 were elevated with LPS treatment in H441 cells. The CCL5 expression from H441 cells in response to 2X concentration of FC and TNFα was beyond the scope of the standard curve and was thus, not included in the graphs (Figure 18b).

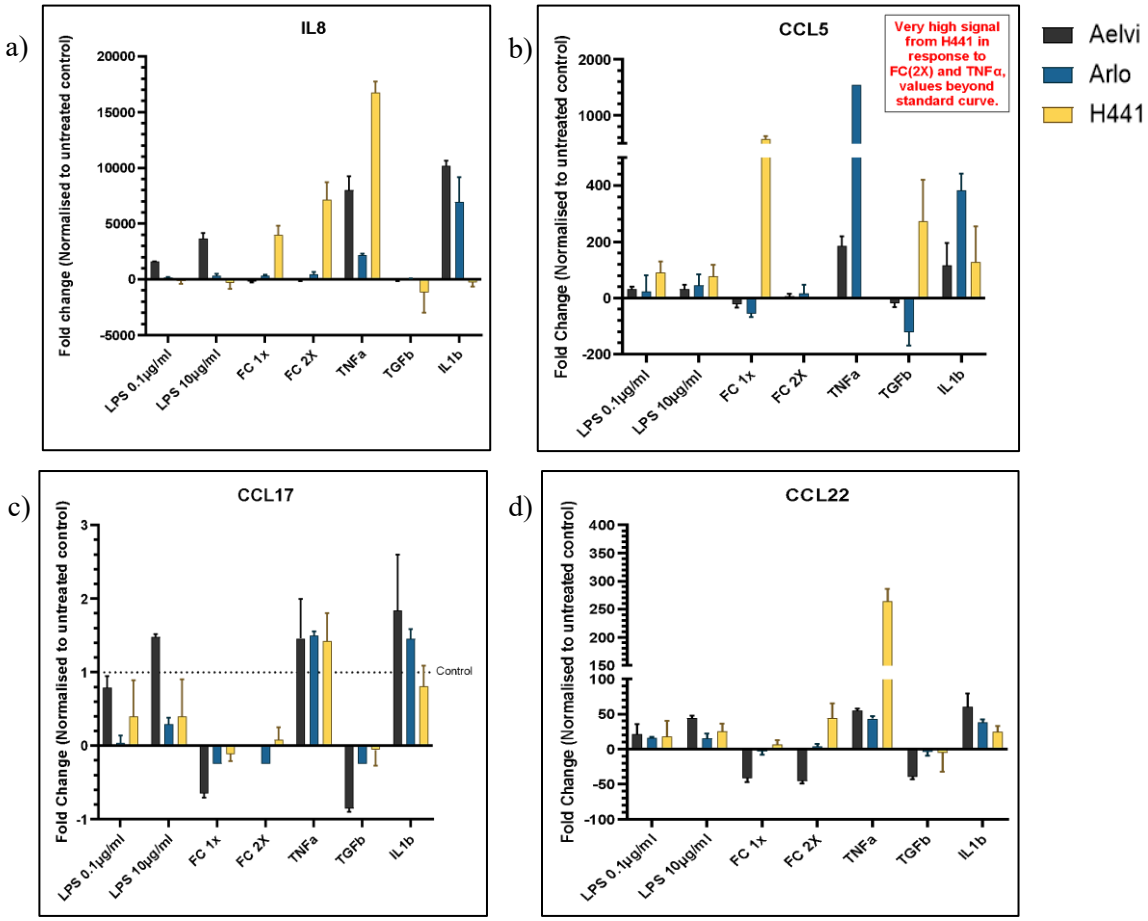

Figure 18. **Chemokine released in response to various inflammatory and fibrotic stimulations.** Chemokine release in the basolateral media post 7-day treatment with LPS (0.1 and 10 µg/ml), Fibrotic cocktail (1X and 2X), TNFα (20ng/ml), TGFβ (10ng/ml), and IL1b (10ng/ml) determined through MSD U-plex assay. Concentrations estimated through standard curve using sigmoidal curve fit with four parameter logistic model in GraphPad PRISM. Resulting concentrations normalized against signal in untreated control. Y-axis range different for each chemokine. (n=3, error bars represent standard deviation). Effect on expression of a) interleukin-8 (IL8) b) C-C motif chemokine ligand-5 (CCL5/RANTES) c) C-C motif chemokine ligand-17(CCL17/TARC), and d) C-C motif chemokine ligand-22 (CCL22/MDC).

The FC containing a mixture of fibrotic factors was used at 1X and 2X concentrations to induce fibrosis. Increased interleukin-6 (IL6) could be detected for Aelvi cells in a dose-dependent manner, and a reduction in chemokine secretion was observed. Arlo cells produced both IL-6 and IL-8 but did not exhibit significant chemokine production. H441 showed a dose-dependent increase in interleukin, GM-CSF, and chemokine production (Figure 19).

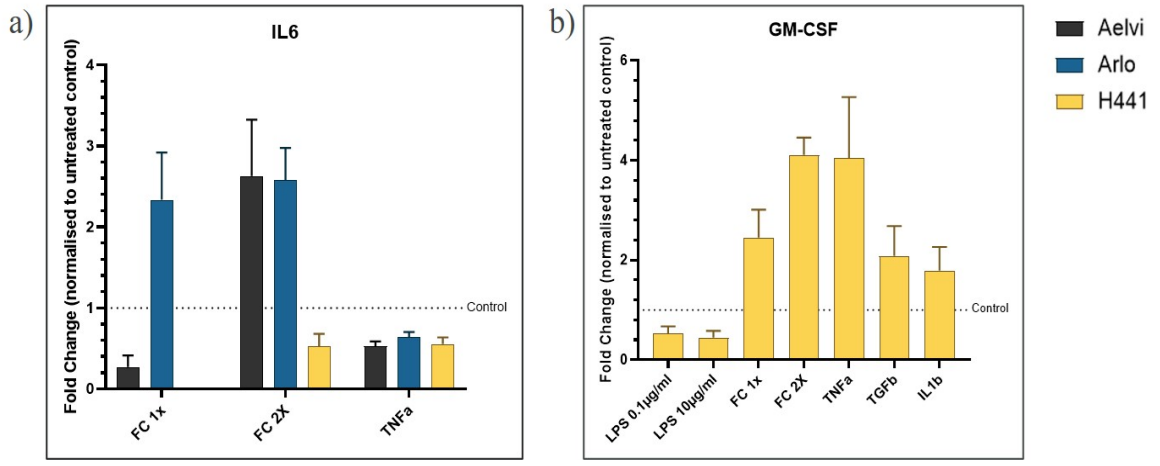

Figure 19. **Interleukin-6 (IL6) and granulocyte-macrophage colony-stimulating factor (GM-CSF) release in response to different stimulations in alveolar ALI models.** Cytokines release in the basolateral media post 7-day treatment with LPS (0.1 and 10 µg/ml), Fibrotic cocktail (1X and 2X), TNFα (20ng/ml), TGFβ (10ng/ml), and IL1β (10ng/ml) determined through MSD U-plex assay. Cytokine concentrations estimated through generation of standard curve using Sigmoidal curve fit with four parameter logistic model in GraphPad PRISM. Resulting concentrations were normalized against signal in untreated control. (n=3, error bars represent standard deviation). a) IL6 expression detected in response to Fibrotic cocktail and TNFα. b) GM-CSF production from H441 cells.

Treatment with TNFα induced secretion of the above-mentioned interleukins and chemokines in all the cell lines. Additionally, H441 showed increased GM-CSF production. TGFβ reduced interleukins and chemokines except CCL5 and GM-CSF in H441 cells. IL1β treatment caused increased chemokine production in the three models. IL6 was not detected. IL8 was increased for Aelvi and Arlo cells but decreased in the H441 model.

Epithelial-Mesenchymal and Aberrant basaloid transition.

Conditions like fibrosis are known to affect the epithelial cell physiology and induce epithelial mesenchymal transformation and manifest aberrant basaloid characters. To investigate these mechanisms, the models were treated with the FC and TGFβ. The RNA samples were collected post 7-day treatment for assessing EMT and AbBa gene expression markers with qPCR.

EMT is linked to increased fibronectin-1 (FN1) and vimentin (VIM) production, in addition to a reduction in junction proteins such as CDH1. All treatments reduced CDH1 levels in Aelvi and Arlo cells whereas H441 showed increased CDH1. Increased VIM and FN1 were observed for Aelvi cells in response to the FC and TGFβ. In the Arlo model, FC induced VIM, and TGFβ induced FN1 (Figure 20).

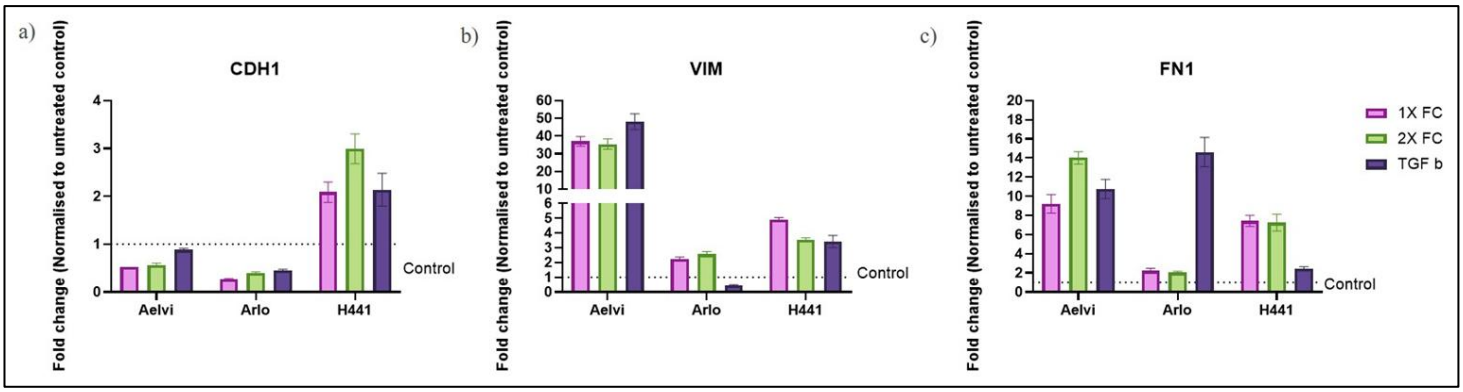

Figure 20. **Epithelial Mesenchymal Transition.** EMT transition gene markers evaluated through Taqman assay (n=3). Change in gene expression determined through fold change (2^ΔΔCT) against untreated control post 7-day treatment with LPS (0.1 and 10 µg/ml), Fibrotic cocktail (1X and 2X), TNFα (20ng/ml), TGFβ(10ng/ml), and IL1β (10ng/ml). Gene expression of a) E-cadherin (CDH1), b) Vimentin (VIM), and c) Fibronectin-1 (FN1).

It is known that matrix metalloproteinase-7 (MMP7) and keratin 17 (KRT17) upregulation is linked to AbBa transition in IPF. FC and TGFβ treatments increased expression of both the genes in Aelvi cells while Arlo and H441 cells showed little to no evidence of AbBa transition (Figure 21).

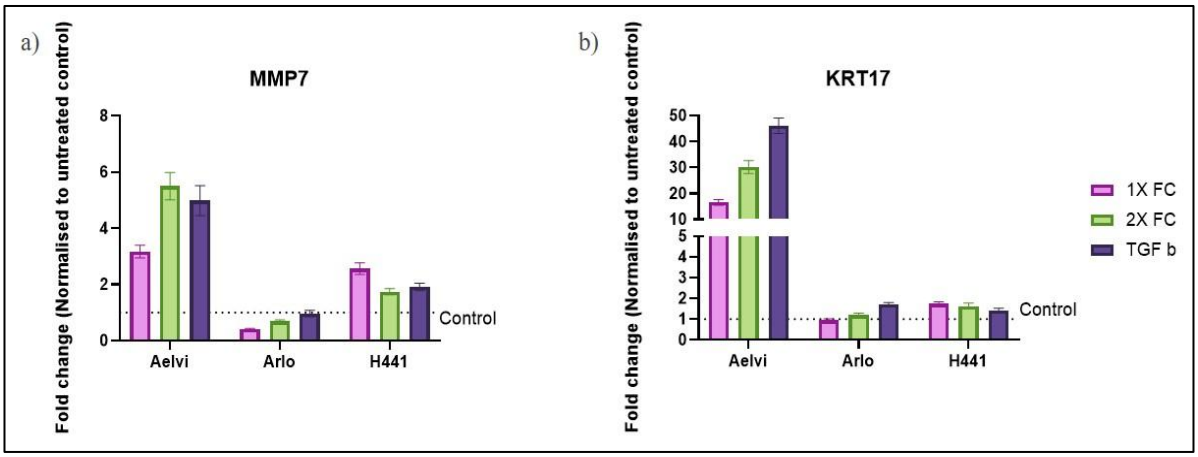

Figure 21. **Aberrant basaloid Transition.** AbBa transition markers checked with Taqman assay (n=3). Change in expression determined through fold change (2^ΔΔCT) against untreated control post 7-day treatment with Fibrotic cocktail (1X and 2X), and TGFβ(10ng/ml). a) Matrix Metalloproteinase-7 (MMP7) expression. b) Keratin 17 (KRT17) expression.

While these results can be evaluated further to generate dose response curves of various treatments, this further emphasizes the functionality of the models to mimic the alveolar biology and disease pathology. More genes associated with EMT and AbBa could be evaluated to further characterise these findings.

Alveolar ALI co-cultures with endothelial cell lines

Endothelial cells from the capillary system are integral components in the air-blood interface. These can produce metabolites that enhance the retention of the natural phenotype of primary

AEC cells in vitro. To check the effect of endothelial cells on the AECs models included in this study, the three models were cultured with different endothelial cell lines growing on the basolateral side of the transwell membrane. Two monoculture wells of each cell AEC cell line – Aelvi, Arlo or H441 were included as a control. Similarly, two wells of each endothelial cell type – Hulec-5a, Huvec or HPMEC, growing on the basolateral side without the epithelial cells were included to monitor the presence of endothelial cells in culture throughout the experiment. Co-culture with endothelial cells did not improve the TEER over time for any of the epithelial cell lines, and in the case of Arlo cells, co-culture even resulted in reduced TEER (Figure 22).

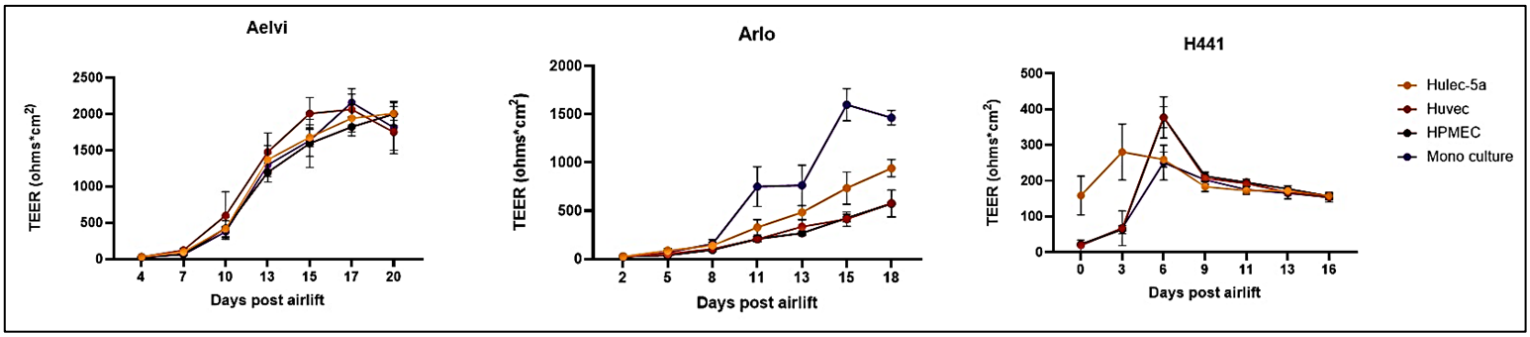

Figure 22. **Effect of co-culture with endothelial cells on the transepithelial electrical resistance (TEER).** The TEER was monitored during co-culture with different endothelial cell lines over 2-3 weeks. The data was adjusted for membrane resistance from an empty well and normalised to area by multiplying with area of the well (monoculture, n=2; co-culture, n=4).

Although direct comparison of the effects of the three endothelial cell lines on the three alveolar ALI models – and with each other – was challenging, it was noted that co-culture with endothelial endothelial cells influences the gene expression of AT1-associated markers (Figure 23) and AT2-associated markers (Figure 24).

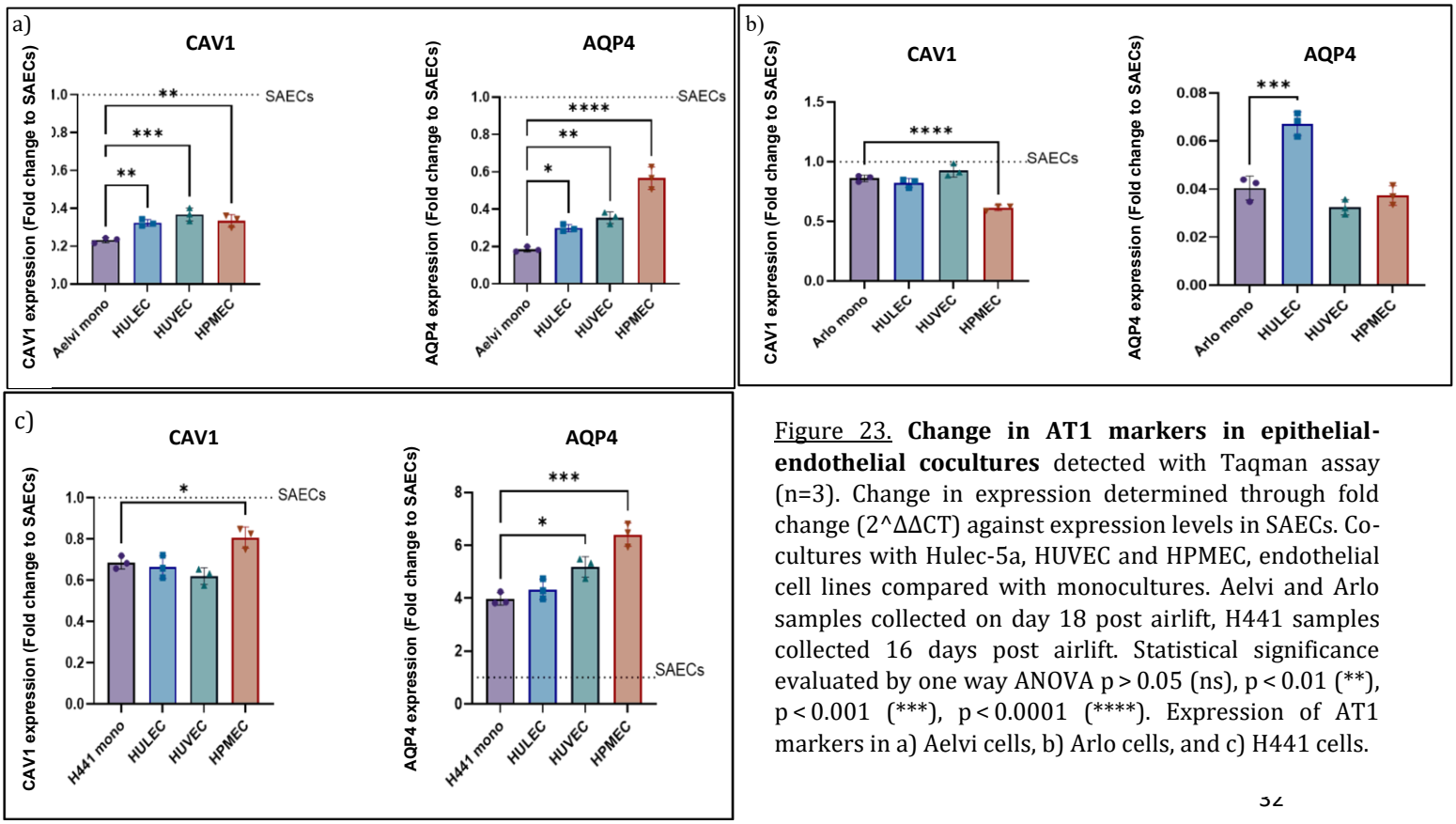

Figure 23. **Change in AT1 markers in epithelial-endothelial cocultures** detected with Taqman assay (n=3). Change in expression determined through fold change (2^ΔΔCT) against expression levels in SAECs. Co-cultures with Hulec-5a, HUVEC and HPMEC, endothelial cell lines compared with monocultures. Aelvi and Arlo samples collected on day 18 post airlift, H441 samples collected 16 days post airlift. Statistical significance evaluated by one way ANOVA $p > 0.05$ (ns), $p < 0.01$ (**), $p < 0.001$ (***), $p < 0.0001$ (****). Expression of AT1 markers in a) Aelvi cells, b) Arlo cells, and c) H441 cells.

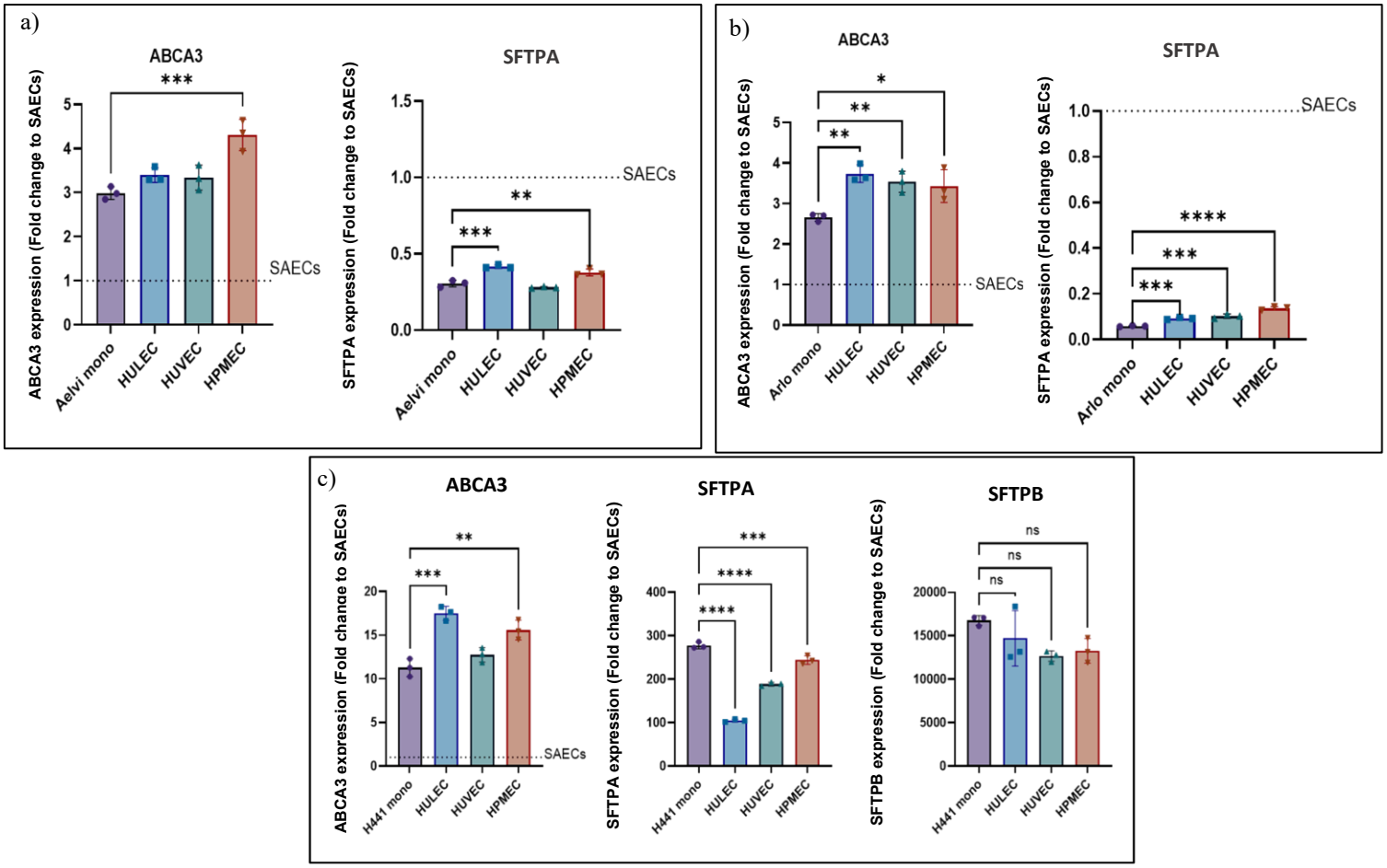

Figure 24. **Change in AT2 cell markers in epithelial-endothelial cocultures** detected with Taqman assay (n=3). Change in expression determined through fold change (2^ΔΔCT) against expression levels in SAECs. Co-cultures with Hulec-5a, HUVEC and HPMEC, endothelial cell lines compared with monocultures. Aelvi and Arlo samples collected on day 18 post airlift, H441 samples collected 16 days post airlift. Statistical significance evaluated by one way ANOVA $p > 0.05$ (ns), $p < 0.01$ (**), $p < 0.001$ (***), $p < 0.0001$ (****). Expression of AT2 markers in a) Aelvi cells, b) Arlo cells, and c) H441 cells.

None of the combinations replicated the AlveolAir model from Epithelix (data not shown), which is a primary cell-based alveolar ALI model. The effect of the co-cultures seemed cell-line as well as target specific. These co-cultures did not significantly improve the readouts for the cell lines in terms of TEER and the marker specific effects would need further characterisation. However, these protocols can serve as a good starting point for cultivating tissue derived primary cells in ALI.

Summarising the different AEC models and their relative strengths.

On comparing the three AEC models based on the different experiments, their relative and variable strengths were determined. Aelvi cells showed the highest TEER with AbBa and EMT markers on treatment with fibrotic stimuli (Figure 20; Figure 21). Arlo cells had a relatively higher TEER as compared to H441 cells. The TEER was highly sensitive to all the different of triggers (Figure 17), as well as co-culture with endothelial cells (Figure 22). H441 cells had a low but stable TEER with evidence of mainly AT2 characters (Figure 12). H441 model also demonstrated immune cell recruitment potential (Figure 18; Figure 19). Thus, preliminary

indications of the different models' suitable applications were made (Table 6). Aelvi model showed potential to mimic the fibrosis pathology, Arlo cells could model barrier disruption and recovery. H441 model could be useful in studying AT2 cell function and immune cell recruitment in injury and infections.

Table 6. **Summary.** Comparison of different AEC models and their application.

	TEER	AEC markers	Cytokine release	Model suitability
Aelvi	2150±145 Ω.cm^2	AT1 and AT2	Average spectrum	Fibrosis model
Arlo	896±160 Ω.cm^2	AT1 and AT2 (Lower than Aelvi)	Low spectrum	Barrier disruption and recovery
H441	250±30 Ω.cm^2	Mainly AT2	Broad spectrum	AT2 cell function, inflammation, and immune cell recruitment.

Discussion

In vitro models mimic biological systems and serve as powerful tools for evaluating cellular behaviour as well as molecular mechanisms underlying health and disease. In this project, three in-vitro air-liquid interface models of the human alveolar barrier were implemented and characterised. The central aim was to evaluate the ability of different immortalised cell-based models for their ability to recapitulate key features of alveolar epithelium including, formation of a strong barrier, and presence of alveolar epithelial cell (AEC) specific markers. Their functionality and translational potential were assessed by exposing them to inflammatory and fibrotic stimuli. Additionally, barrier integrity and epithelial characters were assessed with the ultimate goal of defining the physiological relevance and applicability of these systems to support early drug development and respiratory research.

By utilizing cell lines as opposed to primary tissue-derived cells, the cultures avoided challenges around loss of phenotype in-vitro and ensured a relatively simple and reproducible protocol. Cell lines of cancerous origin (A549 and H441), as well as immortalized healthy cell lines (Alevi and Arlo), were incorporated in this study. A549 and H441 cells are highly referenced as AT2 cells due to their ability to produce junction and surfactant-associated proteins (Selo et al., 2021). However, the cancerous origin of these cell lines can pose limitations in the cellular differentiation and introduce genetic instability. To address this, Aelvi and Arlo cells from the company Inscreenex GmBh were also characterized. These immortalized cell lines are derived from AT1 cells. Recent publications have shown their barrier formation capacity and retention of alveolar epithelial cell markers under ALI conditions. (Carius et al., 2023)

The cell culture protocols for the alveolar basal epithelial cell line A549 have evolved over years to be used as a surrogate for the AT2 cells. In addition to surfactant production, the cells are also used to study drug metabolism, ion transportation, and inflammatory responses (Foster et al., 1998; Barilli et al., 2022). However, A549s fail to produce TEER in ALI cultures. In order to develop a barrier, the cells must differentiate and mature in the culture. The presence of FBS in the routine culture media can keep the cells in a proliferative state limiting their

maturation (Srinivasan et al., 2015; Ross et al., 2021). In the 2022 study from Chary et al., it was shown that transforming A549 cells to FBS free media conditions can improve their AT1 and AT2 characteristics under ALI. To determine whether this protocol could also enhance the barrier formation capacity of these cells, A549 cells were transformed into FBS free CnT Prime Airway media. Despite transformation, the A549s failed to develop TEER (Figure 7d). The cells assumed a thick multi-layered organisation with sparse growth (Figure 7c), in contrast to the compact and thin layers observed in the other cell lines (Figure 9). This indicates that A549s may intrinsically lack the structural and ionic strength required for tight junction formation (Tanabe et al., 2024). While, the cells seemed to grow faster in the CnT media during transformation, their proliferative capacity was reduced post thaw, as also reported by González et al. (2017). The increased proliferation followed by sensitivity to freeze-thaw cycles suggest altered metabolic behaviour rather than a stable phenotypic differentiation and maturation. This reinforces that while A549s may be a useful for metabolic assays, their application in studying epithelial barrier formation remains limited. It is important to note that, the CnT Prime Airway media is supplemented with progenitor targeted growth factors. This could have kept the A549 cells in a proliferative state and limited their maturation potential. (CellnTec Advanced Cell Systems AG). Optimizing the media further with corticosteroids and growth factors aimed at differentiation could possibly help cell maturation towards AEC phenotype (Deng et al., 2022). However, A549's cancerous origin and intrinsic limitations could still challenge such modifications.

In the present study, H441, Aelvi and Arlo cells were further characterised in ALI based on their ability to form a functional barrier. The cell lines required air exposure to form tight junctions and develop a TEER (Figure 9; Figure 10), this proves the physiological relevance of ALI culture technique in the context of alveolar biology. Air exposure mimics the in-vivo environment and provides mechanical cues to help the cells mature and polarise. Removal of apical media creates osmotic and oxygen gradients across the cell layer. These conditions, in addition to apical dehydration, promotes cell polarisation, localisation of junction proteins and cytoskeleton rearrangement. (Tokuda et al., 2019) In submerged cultures, a hypoxic environment develops because the culture medium blocks the oxygen availability to the cell layer. This can promote hypoxia inducible signalling (HIF pathway) and downregulate surfactant production from AT2 cells. In contrast, under ALI conditions, oxygen availability from the apical side enables surfactant production and upregulation of transport channel proteins by preventing HIF signalling (Ito et al., 2011).

Over repeated experiments, Aelvi cells developed the highest TEER reaching 2150±145 Ω.cm2 (Figure 8a), as also described in the literature (Mills-Goodlet et al., 2020). Arlo cells developed a TEER of 896±160 Ω.cm2 (Figure 8b). This is much lower than the Carius et at. (2023) study, where Arlo cells exceeded Aelvi TEER values to reach around 3000 Ω.cm2. This could be due to the difference in the cell culture media used by Carius et at. (2023) where the cultures were maintained in SAGMTM Small Airway Epithelial Cell Growth Medium BulletKit (Lonza #CC-3118). Out of the three cell lines, H441 cells showed the lowest TEER values, 250±30 Ω.cm2 (Figure 8c). This was consistent with 249.3±25.1 Ω.cm2 reported by Munis et al. (2020) whose protocol was adopted in this study. Some protocols also generate lower TEER (166 ± 10 Ω.cm2) for H441 cells (Kalsi et al., 2023). With quantitative differences, all three models produced a stable barrier resistance and restricted transmembrane permeability which shows their potential as an in-vitro model of the alveolar epithelium. The three models were also tested in a 96-well format (data not shown) and the barrier properties were evaluated through FITC-Dextran transmembrane permeability assay. All cell types showed a functional barrier in the 96-well format suggesting the potential for scaling up these models for high-throughput assays.

It is difficult to determine whether a higher TEER value translates to a better model given the limited feasibility to measuring in-vivo TEER from human airways for comparison. Irrespective, all three models developed a stable TEER which can be manipulated in functional assays making them suitable for drug compound testing and efficacy studies.

The AEC gene expression profiles varied between the three cell lines and showed clear differences between the different cell types. As expected, H441 had high expression of AT2 markers, SFTPA, SFTPB, as well as the ion surfactant transporter - ABCA3 in taqman assay. All three markers were many folds higher than in the positive control – AlveolAir (Figure 12). The expression profiles were normalised to ALI cultures of small airway epithelial cells. This was done to obtain a comparative baseline for the three cell lines. Theoretically, SAECs do not express the AT1-AT2 markers, however for the markers presented here, the Ct value threshold was decided and only the markers which produced Ct values of below 32 for SAECs and below 30 for the cell lines were analysed and compared. This is with the exception of SFTPB. For SFTPB the SAECs gave a Ct value of 34, but H441s showed very high expression and thus, this was included in the report. The gene expression profile of H441s remained consistent with the AT2 identity of the cells validating their application in studying secretory function of AT2 cells.

The results show negligible levels of surfactant genes from both Aelvi and Arlo cells and high production of ABCA3 at the transcriptome level (Figure 12). This might indicate a partial lineage commitment from the cell lines; however, immunofluorescent staining confirmed the presence of SFTPB and SPFTPC in Aelvi and Arlo models. This can be attributed to the surfactant homeostasis is the AECs, which is highly controlled through multiple signalling cascades including calcium regulated mechanisms, cAMP and Protein Kinase C (PKC) signalling pathways (Rooney, 2001). Additionally, air exposure, alveolar stretching and autocrine feedback from surfactant proteins (SP-A) and lipid component dipalmitoyl phosphatidylcholine creates feedback inhibition (Olmeda et al., 2017). Considering this, the sample collection protocol for qPCR could have influenced the gene expression levels for the two cell lines. Since the markers were detected with staining against the proteins (SP-C and SP-B) (Figure 14), this reflects the possibility of autocrine feedback limiting transcription of these genes at the time of sample collection (day 18). Running qPCR on samples from multiple timepoints and between media changes might reflect variation in gene expression for surfactants.

To verify the AT1 characters, we explored the gene expression of water channel proteins (aquaporins) and Caveolin 1 (CAV1), out of the five aquaporins (AQP1-5) only AQP3 and AQP4 could be detected with qPCR (Figure 13). The observations further supported the phenotypic differences between the cell lines. H441s showed high levels of AQP4. Though it is not as widely accepted as AQP5 or PDPN for being a true AT1 marker, AQP4 can be found on the basolateral side of the alveolar epithelium (Frigeri et al., 1995). Xiong et al. (2023) have also reported presence of AQP4 in H441 cells. This indicates partial acquisition of AT1 features in the model. Neither of the cell lines showed high levels of CAV1 or AQP3, which could reflect incomplete terminal differentiation but this should be confirmed by running qPCR at intermediate time intervals during ALI cultures. The AT1 markers, AQP5 and PDPN could be detected with confocal imaging (Figure 15). Aelvi cells had the highest expression of both markers among the three cell lines suggesting a mature AT1 phenotype. These observations signal that Aelvi cells best recapitulated AT1 properties.

It is hard to comment on the cellular identity of the different cells in the system without running a more sophisticated analysis like flow cytometry or global mass spectrometry. However, from the observations of this study, it can be assumed that the cells in the ALI cultures would present a mixed population of cells at different stages of differentiation with partial lineage commitment. This heterogeneity likely gives the different models a varying pattern of responsiveness when challenged with inflammatory and fibrotic triggers. It was observed that, Aelvi cells exhibited a decrease in TEER only in response to fibrotic stimuli (fibrotic cocktail and TGFβ), reaffirming the mature epithelial phenotype reactive to remodelling signals. Arlo cells were more sensitive and showed a marked decrease in TEER in response to all stimuli except LPS, indicating potential for modelling epithelial barrier disruption. H441 only reacted to the fibrotic cocktail and TNFα after 3 days of treatment (Figure 17). The culture media for H441 is supplemented with dexamethasone and insulin transferrin selenium which could have had a preventative effect on the barrier integrity in the ALI cultures; thus, the media formulations need to be modified for treatments in this model (Kutsuzawa et al., 2023; Ren Et al., 2016). This emphasizes how the culture conditions shape the model's response to the pathological stimuli, which is an important consideration in assay development.

The increased IL6, GM-CSF and chemokines (IL8, CCL5/17/22) in the basolateral media following 7-day treatment for the different cell lines confirmed the pathological relevance of the models explored in this study (Figure 18; Figure 19). IL6 expression in response to TNFα and fibrotic cocktail indicates acute phase inflammatory responses as seen in COPD and asthma (Rincon & Irvin, 2012). GM-CSF production from H441 cells indicate macrophage activation potential, useful to study bacterial and viral infections (Sever-Chroneos et al., 2011). Increased IL8 marks the epithelial activation and might be useful in modelling neutrophil recruitment and migration studies (Hechtman et al., 1991). Finally, secretion of chemokines CCL5 (RANTES), CCL17 (TARC), and CCL22 (MDC) in the models indicated the potential for method development around epithelial cell mediated adaptive immune engagement and T-cell recruitment in asthma and allergic inflammation (Juremalm et al., 2005; Saeki & Tamaki, 2006). The model's responsiveness to LPS treatment is an important observation, as it supports the use of LPS instead of live bacteria in neutrophil transepithelial migration models, as well as in studies of infections and alveolar macrophage activation.

While not thoroughly characterised in this study, epithelial-mesenchymal (EMT) and aberrant basaloid (AbBa) transition was also demonstrated in response to fibrotic treatments (Figure 20; Figure 21). EMT plays an important role in tissue regeneration and embryonic development (Kalluri & Weinberg, 2009). AbBa cells are epithelial cells that adopt a basaloid phenotype during lung fibrosis (Hoffman et al., 2024). More recently, these cellular transition mechanisms have been shown to drive tumor metastasis and have emerged as therapeutic targets for progressive lung diseases like COPD and IPF (Zheng et al., 2025). The models characterised in this project, especially the Aelvi model showed high responsiveness to fibrotic triggers. This could be developed further to study these mechanisms for tissue remodelling in IPF.

These findings emphasize the relevance and suitability of the cell line-based ALI models in alveolar in-vitro biology. Supporting the central hypothesis of this project, we showed that the immortalised cell-line based models developed and maintained key characters of alveolar epithelial cells including a functional TEER, AEC markers, and responsiveness to inflammatory and fibrotic treatments. This study compared the three most common cell-based models and demonstrated their variable strengths and suitability in answering different research questions, as summarised in Table 6. H441 can serve as a simple and functional model of AT2 cells. Aelvi cells represented mixed AT1- AT2 population, and can be used to model fibrosis.

Arlo cells are the most recently established cell line and retain both AT1 and AT2 markers, albeit at lower levels than Aelvi cells. However, their heightened sensitivity in TEER measurements can be advantageous for studying barrier integrity loss in response to inflammation and injury, as well as its recovery following treatment with therapeutic candidates.

These systems serve as a good starting point for alveolar in-vitro modelling and can also easily cultivate more cell types, such as, immune cells and endothelial cells model alveolar complexity more closely (Kletting et al., 2018). However, to increase the translational potential of these models, further exploration of endothelial, and ECM components alongside fibroblasts is vital. Nevertheless, the cell lines-based models characterised in this project are highly scalable and provide experimental control and flexibility, which are key features to generate reproducible data. The functional potential of these models is invaluable in exploring alveolar biology and uncovering molecular mechanisms. Through further characterisation of the individual cell lines with more global proteomic and genomic approaches, the cell line specific variations can be manipulated to produce tailored models that address either disease specific or biological questions.

The success of these cultures in forming a functional barrier while retaining AEC characters proves their suitability for early-stage translational research and drug disposition studies. With further characterisations, and exploration of multi-cellular co-cultures, these cell lines can provide the foundation for developing more sophisticated systems involving primary cells and induced pluripotent stem cell derived AECs that potentially replicates alveolar complexity in more physiological relevant manner ultimately driving alveolar model development towards bridging in-vitro research with clinical relevance.

References

1. Abo, K. M., Sainz de Aja, J., Lindstrom-Vautrin, J., Alysandratos, K. D., Richards, A., Garcia-de-Alba, C., Huang, J., Hix, O. T., Werder, R. B., Bullitt, E., Hinds, A., Falconer, I., Villacorta-Martin, C., Jaenisch, R., Kim, C. F., Kotton, D. N., & Wilson, A. A. (2022). Air-liquid interface culture promotes maturation and allows environmental exposure of pluripotent stem cell-derived alveolar epithelium. *JCI Insight, 7*(6), e155589. https://doi.org/10.1172/jci.insight.155589
2. Augusto, L. A., Synguelakis, M., Johansson, J., & Chaby, R. (2003). Interaction of pulmonary surfactant protein C with CD14 and lipopolysaccharide. *Infection and Immunity, 71*(1), 61–67. https://doi.org/10.1128/iai.71.1.61-67.2003
3. Augusto, L. A., Li, J., Synguelakis, M., Johansson, J., & Chaby, R. (2002). Structural basis for interactions between lung surfactant protein C and bacterial lipopolysaccharide. *Journal of Biological Chemistry, 277*(26), 23484–23492. https://doi.org/10.1074/jbc.M200939200
4. Balest, A. L. (2023, July 3). Overview of perinatal respiratory disorders. *MSD Manual Professional Edition*. https://www.msdmanuals.com/professional/pediatrics/respiratory-problems-in-neonates/overview-of-perinatal-respiratory-disorders
5. Barilli, A., Visigalli, R., Ferrari, F., Bianchi, M. G., Dall'Asta, V., & Rotoli, B. M. (2022). Immune-mediated inflammatory responses of alveolar epithelial cells: Implications for COVID-19 lung pathology. *Biomedicines, 10*(3), 618. https://doi.org/10.3390/biomedicines10030618
6. Beers, M. F., & Moodley, Y. (2017). When Is an Alveolar Type 2 Cell an Alveolar Type 2 Cell? A Conundrum for Lung Stem Cell Biology and Regenerative Medicine. *American Journal of Respiratory Cell and Molecular Biology*, 57(1), 18–27. https://doi.org/10.1165/rcmb.2016-0426ps
7. Brandt, J. P., & Mandiga, P. (2023). Histology, Alveolar Cells. PubMed; StatPearls Publishing. https://www.ncbi.nlm.nih.gov/books/NBK557542/
8. Campiglio, C. E., Figliuzzi, M., Silvani, S., Tironi, M., Conti, S., Boschetti, F., & Remuzzi, A. (2021). Influence of culture substrates on morphology and function of pulmonary alveolar cells *in vitro*. *Biomolecules, 11*(5), 675. https://doi.org/10.3390/biom11050675
9. Carius, P., Jungmann, A., Bechtel, M., Grißmer, A., Boese, A., Gasparoni, G., Salhab, A., Seipelt, R., Urbschat, K., Richter, C., Meier, C., Bojkova, D., Cinatl, J., Walter, J., Schneider-Daum, N., & Lehr, C.-M. (2023). A monoclonal human alveolar epithelial cell line ("Arlo") with pronounced barrier function for studying drug permeability and viral infections. *Advanced Science, 10*(8), e2207301. https://doi.org/10.1002/advs.202207301
10. CellnTec Advanced Cell Systems AG. (n.d.). *CNT-PR-A: Airway epithelial progenitor medium*. CellnTec. https://cellntec.com/products/cnt-pr-a/
11. Chary, A., Groff, K., Stucki, A. O., Contal, S., Stoffels, C., Cambier, S., Sharma, M., Gutleb, A. C., & Clippinger, A. J. (2022). Maximizing the relevance and reproducibility of A549

cell culture using FBS-free media. *Toxicology in Vitro, 83*, 105423. https://doi.org/10.1016/j.tiv.2022.105423

12. Chaudhry, R., Omole, A. E., & Bordoni, B. (2024). Anatomy, thorax, lungs. In *StatPearls* [Internet]. StatPearls Publishing. https://www.ncbi.nlm.nih.gov/books/NBK470197/
13. Chua, F., & Laurent, G. J. (2006). Fibroblasts. In G. J. Laurent & S. D. Shapiro (Eds.), *Encyclopedia of respiratory medicine* (pp. 213–219). Academic Press. https://doi.org/10.1016/B0-12-370879-6/00156-3
14. Chuquimia, O. D., Petursdottir, D. H., Periolo, N., & Fernández, C. (2013). Alveolar epithelial cells are critical in protection of the respiratory tract by secretion of factors able to modulate the activity of pulmonary macrophages and directly control bacterial growth. *Infection and Immunity, 81*(1), 381–389. https://doi.org/10.1128/IAI.00950-12
15. CI-Arlo. (2025, July 3). *Immortalized human alveolar epithelial cells: Product sheet*. InScreenEx GmbH. https://www.inscreenex.de/wp-content/uploads/2024/05/inscreenex-Product-Sheet-huArlo-INS-CI-1031.pdf
16. CI-hAELVi. (2025, July 3). *Immortalized human alveolar epithelial cells: Product sheet*. InScreenEx GmbH. https://www.inscreenex.de/wp-content/uploads/2024/05/inscreenex-Product-Sheet-hAELVi-INS-CI-1015.pdf
17. Corrin, B., Nicholson, A. G., Burke, M. M., & Rice, A. (2011). Pathology of the lungs. Churchill Livingstone/Elsevier.
18. Creuwels, L. A., van Golde, L. M., & Haagsman, H. P. (1997). The pulmonary surfactant system: Biochemical and clinical aspects. Lung, 175(1), 1–39. https://doi.org/10.1007/pl00007554
19. Deng, H., Gao, Y., Trappetti, V., Hertig, D., Karatkevich, D., Losmanova, T., Urzi, C., Ge, H., Geest, G. A., Bruggmann, R., Djonov, V., Nuoffer, J. M., Vermathen, P., Zamboni, N., Riether, C., Ochsenbein, A., Peng, R. W., Kocher, G. J., Schmid, R. A., Dorn, P., & Marti, T. M. (2022). Targeting lactate dehydrogenase B-dependent mitochondrial metabolism affects tumor initiating cells and inhibits tumorigenesis of non-small cell lung cancer by inducing mtDNA damage. *Cellular and Molecular Life Sciences, 79*(8), 445. https://doi.org/10.1007/s00018-022-04453-5
20. Evans, K. V., & Lee, J. H. (2020). Alveolar wars: The rise of in vitro models to understand human lung alveolar maintenance, regeneration, and disease. *Stem Cells Translational Medicine,* 9(8), 867–881. https://doi.org/10.1002/sctm.19-0433
21. EVOM Epithelial Volt/Ohm (TEER) Meter 3. (2019). Wpiinc.com. https://www.wpiinc.com/evom3-epithelial-volt-ohm-teer-meter-3.html
22. *Evotip PURE*. (2024, May 17). Evosep Biosystems. https://www.evosep.com/evotip/
23. Foster, K. A., Oster, C. G., Mayer, M. M., Avery, M. L., & Audus, K. L. (1998). Characterization of the A549 cell line as a type II pulmonary epithelial cell model for drug metabolism. *Experimental Cell Research, 243*(2), 359–366. https://doi.org/10.1006/excr.1998.4172
24. Frigeri, A., Gropper, M. A., Turck, C. W., & Verkman, A. S. (1995). Immunolocalization of the mercurial-insensitive water channel and glycerol intrinsic protein in epithelial cell plasma membranes. *Proceedings of the National Academy of Sciences of the United States of America, 92*(10), 4328–4331. https://doi.org/10.1073/pnas.92.10.4328

25. Gehr, P., Bachofen, M., & Weibel, E. R. (1978). The normal human lung: Ultrastructure and morphometric estimation of diffusion capacity. *Respiratory Physiology*, 32(2), 121–140. https://doi.org/10.1016/0034-5687(78)90104-4
26. Ghonim, M. A., Boyd, D. F., Flerlage, T., & Thomas, P. G. (2023). Pulmonary inflammation and fibroblast immunoregulation: From bench to bedside. *Journal of Clinical Investigation, 133*(17), e170499. https://doi.org/10.1172/JCI170499
27. Gonzalez RF, Allen L, Gonzales L, Ballard PL, Dobbs LG (2010). HTII-280, a biomarker specific to the apical plasma membrane of human lung alveolar type II cells. *J Histochem Cytochem, 58(10), 891-901*. https://doi.org/10.1369/jhc.2010.956433.
28. González, S., Chen, L., & Deng, S. X. (2017). Comparative study of xenobiotic-free media for the cultivation of human limbal epithelial stem/progenitor cells. *Tissue Engineering Part C: Methods, 23*(4), 219–227. https://doi.org/10.1089/ten.tec.2016.0388
29. Guillot, L., Nathan, N., Tabary, O., Thouvenin, G., Le Rouzic, P., Corvol, H., Amselem, S., & Clement, A. (2013). Alveolar epithelial cells: Master regulators of lung homeostasis. *International Journal of Biochemistry & Cell Biology, 45*(11), 2568–2573. https://doi.org/10.1016/j.biocel.2013.08.009
30. Han, S., & Mallampalli, R. K. (2015). The role of surfactant in lung disease and host defense against pulmonary infections. *Annals of the American Thoracic Society, 12*(5), 765–774. https://doi.org/10.1513/AnnalsATS.201411-507FR
31. Hechtman, D. H., Cybulsky, M. I., Fuchs, H. J., Baker, J. B., & Gimbrone, M. A., Jr. (1991). Intravascular IL-8: Inhibitor of polymorphonuclear leukocyte accumulation at sites of acute inflammation. *Journal of Immunology, 147*(3), 883–892. https://doi.org/10.1046/j.1523-1755.1999.055003852.x
32. Herrero, R., & Matute-Bello, G. (2015). How to measure alterations in alveolar barrier function as a marker of lung injury. *Current Protocols in Toxicology, 63*(1), 24.3.1–24.3.15. https://doi.org/10.1002/0471140856.tx2403s63
33. High-Capacity cDNA Reverse Transcription Kit. (2024). Thermofisher.com. https://www.thermofisher.com/order/catalog/product/4374966
34. Hoffman, E. T., Barboza, W. R., Rodriguez, L. R., Dherwani, R., Tomer, Y., Murthy, A., Bennett, A., Nottingham, A., Babu, A., Chavez, K., Cooper, C. H., Basil, M. C., Raredon, M. S. B., & Katzen, J. (2024). Aberrant transitional alveolar epithelial cells promote pathogenic activation of lung fibroblasts in preclinical fibrosis modeling. *bioRxiv*. https://doi.org/10.1101/2024.06.17.599351
35. Hogan, B. L., Barkauskas, C. E., Chapman, H. A., Epstein, J. A., Jain, R., Hsia, C. C., Niklason, L., Calle, E., Le, A., Randell, S. H., Rock, J., Snitow, M., Krummel, M., Stripp, B. R., Vu, T., White, E. S., Whitsett, J. A., & Morrisey, E. E. (2014). Repair and regeneration of the respiratory system: Complexity, plasticity, and mechanisms of lung stem cell function. *Cell Stem Cell, 15*(2), 123–138. https://doi.org/10.1016/j.stem.2014.07.012
36. Hollenhorst, M. I., Richter, K., & Fronius, M. (2011). Ion transport by pulmonary epithelia. *Journal of Biomedicine and Biotechnology, 2011*, 174-306. https://doi.org/10.1155/2011/174306
37. Ito, Y., Ahmad, A., Kewley, E., & Mason, R. J. (2011). Hypoxia-inducible factor regulates expression of surfactant protein in alveolar type II cells in vitro. *American Journal of*

Respiratory Cell and Molecular Biology, 45(5), 938–945. https://doi.org/10.1165/rcmb.2011-0052OC

38. Jiang, D., Schaefer, N., & Chu, H. W. (2018). Air-liquid interface culture of human and mouse airway epithelial cells. In H. W. Chu (Ed.), *Lung innate immunity and inflammation: Methods and protocols,* 91–109. Humana Press. https://doi.org/10.1007/978-1-4939-8570-8_8
39. Juremalm, M., Olsson, N., & Nilsson, G. (2005). CCL17 and CCL22 attenuate CCL5-induced mast cell migration. *Clinical & Experimental Allergy, 35*(6), 708–712. https://doi.org/10.1111/j.1365-2222.2005.02203.x
40. Kalluri, R., & Weinberg, R. A. (2009). The basics of epithelial-mesenchymal transition. *Journal of Clinical Investigation, 119*(6), 1420–1428. https://doi.org/10.1172/JCI39104
41. Kalsi, K. K., Jackson, S., & Baines, D. L. (2023). Lipoxin receptor agonist and inhibition of LTA4 hydrolase prevent tight junction disruption caused by *P. aeruginosa* filtrate in airway epithelial cells. *PLoS ONE, 18*(7), e0287183. https://doi.org/10.1371/journal.pone.0287183
42. Kapałczyńska, M., Kolenda, T., Przybyła, W., Zajączkowska, M., Teresiak, A., Filas, V., Ibbs, M., Bliźniak, R., Łuczewski, Ł., & Lamperska, K. (2018). 2D and 3D cell cultures: A comparison of different types of cancer cell cultures. *Archives of Medical Science, 14*(4), 910–919. https://doi.org/10.5114/aoms.2016.63743
43. Kemp, S. J., Thorley, A. J., Gorelik, J., Seckl, M. J., O'Hare, M. J., Arcaro, A., Korchev, Y., Goldstraw, P., & Tetley, T. D. (2008). Immortalization of human alveolar epithelial cells to investigate nanoparticle uptake. *American Journal of Respiratory Cell and Molecular Biology, 39*(5), 591–597. https://doi.org/10.1165/rcmb.2007-0334OC
44. Khan, Y. S., & Carey, F. J. (2025, April 6). Histology, lung. In *StatPearls* [Internet]. StatPearls Publishing. https://www.ncbi.nlm.nih.gov/books/NBK534789/
45. Kia'i, N., & Bajaj, T. (2019). Histology, respiratory epithelium. In *StatPearls* [Internet]. StatPearls Publishing. https://www.ncbi.nlm.nih.gov/books/NBK541061/
46. Knudsen, L., & Ochs, M. (2018). The micromechanics of lung alveoli: Structure and function of surfactant and tissue components. *Histochemistry and Cell Biology, 150*(6), 661–676. https://doi.org/10.1007/s00418-018-1747-9
47. Korrodi-Gregório, L., Soto-Cerrato, V., Vitorino, R., Fardilha, M., & Pérez-Tomás, R. (2016). From proteomic analysis to potential therapeutic targets: Functional profile of two lung cancer cell lines, A549 and SW900, widely studied in pre-clinical research. *PLoS ONE, 11*(11), e0165973. https://doi.org/10.1371/journal.pone.0165973
48. Kuehn, A., et al. (2016). Human alveolar epithelial cells expressing tight junctions to model the air-blood barrier. *ALTEX, 33*(3), 251–260. https://doi.org/10.14573/altex.1511131
49. Kulak, N., Pichler, G., Paron, I. *et al.* Minimal, encapsulated proteomic-sample processing applied to copy-number estimation in eukaryotic cells. *Nat Methods* **11**, 319–324 (2014). https://doi.org/10.1038/nmeth.2834
50. Kulkarni, T., de Andrade, J., Zhou, Y., Luckhardt, T., & Thannickal, V. J. (2016). Alveolar epithelial disintegrity in pulmonary fibrosis. *American Journal of Physiology-Lung Cellular and Molecular Physiology, 311*(2), 185–191. https://doi.org/10.1152/ajplung.00115.2016

51. Kutsuzawa, N., Ito, Y., Kagawa, S., Kohno, C., Takiguchi, H., & Asano, K. (2023). Dexamethasone restores TNFα-induced epithelial barrier dysfunction in primary rat alveolar epithelial cells. *PLoS ONE, 18*(12), 295-684. https://doi.org/10.1371/journal.pone.0295684
52. Leibel, S.L., Winquist, A., Tseu, I. *et al.* Reversal of Surfactant Protein B Deficiency in Patient Specific Human Induced Pluripotent Stem Cell Derived Lung Organoids by Gene Therapy. *Sci Rep* **9**, 13450 (2019). https://doi.org/10.1038/s41598-019-49696-8
53. Lieber, M., Smith, B., Szakal, A., Nelson-Rees, W., & Todaro, G. (1976). A continuous tumor-cell line from a human lung carcinoma with properties of type II alveolar epithelial cells. *International Journal of Cancer, 17*(1), 62–70. https://doi.org/10.1002/ijc.2910170110
54. Liu, Y., Wu, P., Wang, Y., Liu, Y., Yang, H., Zhou, G., Wu, X., & Wen, Q. (2022). Application of precision-cut lung slices as an in vitro model for research of inflammatory respiratory diseases. Bioengineering, 9(12), 767. https://doi.org/10.3390/bioengineering9120767
55. Lochbaum, R., Schilpp, C., Nonnenmacher, L., Frick, M., Dietl, P., & Wittekindt, O. H. (2020). Retinoic acid signalling adjusts tight junction permeability in response to air-liquid interface conditions. *Cell Signalling, 65,* 109421. https://doi.org/10.1016/j.cellsig.2019.109421
56. Lopes, C. F., Laurent, E., Caul-Futy, M., Dubois, J., Mialon, C., Chojnacki, C., Sage, E., Boda, B., Huang, S., Rosa-Calatrava, M., & Constant, S. (2025). A novel in vitro primary human alveolar model (AlveolAir™) for H1N1 and SARS-CoV-2 infection and antiviral screening. *Microorganisms, 13*(3), 572. https://doi.org/10.3390/microorganisms13030572
57. Lucas, R., Verin, A. D., Black, S. M., & Catravas, J. D. (2009). Regulators of endothelial and epithelial barrier integrity and function in acute lung injury. *Biochemical Pharmacology, 77*(12), 1763–1772. https://doi.org/10.1016/j.bcp.2009.01.014
58. Maitra, M., Wang, Y., Gerard, R. D., Mendelson, C. R., & Garcia, C. K. (2010). Surfactant protein A2 mutations associated with pulmonary fibrosis lead to protein instability and endoplasmic reticulum stress. *Journal of Biological Chemistry, 285*(29), 22103–22113. https://doi.org/10.1074/jbc.M110.121467
59. Martin, T. R. (2000). Recognition of Bacterial Endotoxin in the Lungs. *American Journal of Respiratory Cell and Molecular Biology*, *23*(2), 128–132. https://doi.org/10.1165/ajrcmb.23.2.f189
60. Mills-Goodlet, R., Schenck, M., Chary, A., Geppert, M., Serchi, T., Hofer, S., Hofstätter, N., Feinle, A., Hüsing, N., Gutleb, A. C., Himly, M., & Duschl, A. (2020). Biological effects of allergen–nanoparticle conjugates: Uptake and immune effects determined on hAELVi cells under submerged vs. air–liquid interface conditions. *Environmental Science: Nano, 7*(7), 2073–2086. https://doi.org/10.1039/C9EN01353A
61. Ochs, M., Nyengaard, J. R., Jung, A., Knudsen, L., Voigt, M., Wahlers, T., Richter, J., & Gundersen, H. J. (2004). The number of alveoli in the human lung. *American Journal of Respiratory and Critical Care Medicine, 169*(1), 120–124. https://doi.org/10.1164/rccm.200308-1107OC

62. Olmeda, B., Martínez-Calle, M., & Pérez-Gil, J. (2017). Pulmonary surfactant metabolism in the alveolar airspace: Biogenesis, extracellular conversions, recycling. *Annals of Anatomy, 209*, 78–92. https://doi.org/10.1016/j.aanat.2016.09.008
63. Penkala, I. J., Liberti, D. C., Pankin, J., Sivakumar, A., Kremp, M. M., Jayachandran, S., Katzen, J., Leach, J. P., Windmueller, R., Stolz, K., Morley, M. P., Babu, A., Zhou, S., Frank, D. B., & Morrisey, E. E. (2021). Age-dependent alveolar epithelial plasticity orchestrates lung homeostasis and regeneration. *Cell Stem Cell, 28*(10), 1775–1789.e5. https://doi.org/10.1016/j.stem.2021.04.026
64. Ptasinski, V., Monkley, S. J., Öst, K., Tammia, M., Alsafadi, H. N., Overed-Sayer, C., Hazon, P., Wagner, D. E., & Murray, L. A. (2023). Modeling fibrotic alveolar transitional cells with pluripotent stem cell-derived alveolar organoids. *Life Science Alliance, 6*(8), e202201853. https://doi.org/10.26508/lsa.202201853
65. Rashid, A. A., & El-Sheikh, A. A. (2025). Exploring the frontier of lung alveolar regeneration: Cellular dynamics, aging effects, and emerging therapeutics. *Translational Research in Anatomy, 40*, 100411. https://doi.org/10.1016/j.tria.2025.100411
66. Reid, R., Roberts, F., & Macduff, E. (2011). Pathology illustrated. Elsevier/Churchill Livingstone.https://www.sciencedirect.com/science/article/abs/pii/B9780702033766500121
67. Ren, H., Birch, N. P., & Suresh, V. (2016). An optimised human cell culture model for alveolar epithelial transport. *PLoS ONE, 11*(10), e0165225. https://doi.org/10.1371/journal.pone.0165225
68. Rincon, M., & Irvin, C. G. (2012). Role of IL-6 in asthma and other inflammatory pulmonary diseases. *International Journal of Biological Sciences, 8*(9), 1281–1290. https://doi.org/10.7150/ijbs.4874
69. RNeasy Plus Kits. (2015). Www.qiagen.com. https://www.qiagen.com/us/products/discovery-and-translational-research/dna-rna-purification/rna-purification/total-rna/rneasy-plus-kits
70. Rooney, S. A. (2001). Regulation of surfactant secretion. *Comparative Biochemistry and Physiology Part A: Molecular & Integrative Physiology, 129*(1), 233–243. https://doi.org/10.1016/s1095-6433(01)00320-8
71. Ross, A. M., Walsh, D. R., Cahalane, R. M., Marcar, L., & Mulvihill, J. J. E. (2021). The effect of serum starvation on tight junctional proteins and barrier formation in Caco-2 cells. *Biochemistry and Biophysics Reports, 27*, 101096. https://doi.org/10.1016/j.bbrep.2021.101096
72. Saeki, H., & Tamaki, K. (2006). Thymus and activation regulated chemokine (TARC)/CCL17 and skin diseases. *Journal of Dermatological Science, 43*(2), 75–84. https://doi.org/10.1016/j.jdermsci.2006.06.002
73. Salomon, J. J., Muchitsch, V. E., Gausterer, J. C., Schwagerus, E., Huwer, H., Daum, N., Lehr, C. M., & Ehrhardt, C. (2014). The cell line NCl-H441 is a useful *in vitro* model for transport studies of human distal lung epithelial barrier. *Molecular Pharmaceutics, 11*(3), 995–1006. https://doi.org/10.1021/mp4006535
74. Selo, M. A., Sake, J. A., Kim, K.-J., & Ehrhardt, C. (2021). *In vitro and ex vivo models in inhalation biopharmaceutical research—Advances, challenges and future perspectives*.

Advanced Drug Delivery Reviews, 176, 113862. https://doi.org/10.1016/j.addr.2021.113862
75. Sever-Chroneos, Z., Murthy, A., Davis, J., Florence, J. M., Kurdowska, A., Krupa, A., Tichelaar, J. W., White, M. R., Hartshorn, K. L., Kobzik, L., Whitsett, J. A., & Chroneos, Z. C. (2011). GM-CSF modulates pulmonary resistance to influenza A infection. *Antiviral Research, 92*(2), 319–328. https://doi.org/10.1016/j.antiviral.2011.08.022
76. Shulenin, S., Nogee, L. M., Annilo, T., Wert, S. E., Whitsett, J. A., & Dean, M. (2004). ABCA3 gene mutations in newborns with fatal surfactant deficiency. *New England Journal of Medicine, 350*(13), 1296–1303. https://doi.org/10.1056/NEJMoa032178
77. Tanabe, I., Ishimori, K., & Ishikawa, S. (2024). Development of an in vitro human alveolar epithelial air–liquid interface model using a small molecule inhibitor cocktail. *BMC Molecular and Cell Biology, 25* (9). https://doi.org/10.1186/s12860-024-00590-7
78. ThermoFisher Scientific. (2024) TrypLE Select User Guide. Available at: https://assets.thermofisher.com/TFS-Assets/LSG/manuals/MAN0019355_TrypLE_Select_UG.pdf.
79. Tokuda, S., & Yu, A. S. L. (2019). Regulation of Epithelial Cell Functions by the Osmolality and Hydrostatic Pressure Gradients: A Possible Role of the Tight Junction as a Sensor. *International Journal of Molecular Sciences*, *20*(14), 3513. https://doi.org/10.3390/ijms20143513
80. Trapnell BC, Whitsett JA, Nakata K. Pulmonary alveolar proteinosis. N Engl J Med. 2003 Dec 25;349(26):2527-39. doi: 10.1056/NEJMra023226
81. Rapnell, B. C., Whitsett, J. A., & Nakata, K. (2003). Pulmonary alveolar proteinosis. *New England Journal of Medicine, 349*(26), 2527–2539. https://doi.org/10.1056/NEJMra023226
82. *U-PLEX Custom Biomarker Group 1 (human) Assays | Meso Scale Discovery*. (2023). Mesoscale.com. https://www.mesoscale.com/en/products/u-plex-custom-biomarker-human-assays-k15067m/
83. Vazquez-Armendariz, A. I., & Tata, P. R. (2023). Recent advances in lung organoid development and applications in disease modeling. *Journal of Clinical Investigation, 133*(22), e170500. https://doi.org/10.1172/JCI170500
84. Ware, L. B., & Matthay, M. A. (2001). Alveolar fluid clearance is impaired in the majority of patients with acute lung injury and the acute respiratory distress syndrome. *American Journal of Respiratory and Critical Care Medicine, 163*, 1376–1383. https://doi.org/10.1056/NEJMra023226
85. Weibel, E. R., Sapoval, B., & Filoche, M. (2005). Design of peripheral airways for efficient gas exchange. *Respiratory Physiology & Neurobiology, 148*(1–2), 3–21. https://doi.org/10.1016/j.resp.2005.03.005
86. Whitsett, J. A., Wert, S. E., & Weaver, T. E. (2010). Alveolar surfactant homeostasis and the pathogenesis of pulmonary disease. *Annual Review of Medicine, 61*, 105–119. https://doi.org/10.1146/annurev.med.60.041807.123500
87. Xiong, J., Kaleja, P., Ückert, L., Nezaratizadeh, N., Krantz, S., Krause, M. F., Fitschen-Oestern, S., Seekamp, A., Cassidy, L., Tholey, A., & Fuchs, S. (2023). Alveolar-capillary barrier protection in vitro: Lung cell type-specific effects and molecular mechanisms

induced by 1α,25-dihydroxyvitamin D_3. *International Journal of Molecular Sciences, 24*(8), 7298. https://doi.org/10.3390/ijms24087298

88. Yang, J., et al. (2016). The development and plasticity of alveolar type 1 cells. *Development, 143*(1), 54–65. https://doi.org/10.1242/dev.130005
89. Zheng, C., Zhang, L., Sun, Y., Ma, Y., & Zhang, Y. (2025). Alveolar epithelial cell dysfunction and epithelial-mesenchymal transition in pulmonary fibrosis pathogenesis. *Frontiers in Molecular Biosciences, 12*, 1564176. https://doi.org/10.3389/fmolb.2025.1564176

Acknowledgements

I am deeply thankful to Lund University and AstraZeneca R&D, Gothenburg for giving me the opportunity to perform and produce this work for my master thesis. I sincerely thank my supervisors Jenny Horndahl and Linda Yrlid for their continued guidance and support throughout the project time frame. Thank you to my university supervisor Olivier Van Aken and examiner Marita Cohn for their timely guidance from time to time, and my course coordinator Cristina Ledje for her continued support with the administrative formalities. This work has been possible due to the continued technical help from several colleagues from AstraZeneca's COPD-IPF department at Gothenburg.

I would also like to thank the external collaborators from Inscrenex Gmbh, Germany for providing the cell licences and their support during this time. Special thanks to Nicole Schneider-Daum from Helmholtz-Institut für Pharmazeutische Forschung Saarland, Saarbrücken, Germany for sharing her insights on working with Arlo and Aelvi cells. I deeply appreciate the MSD support team from the United States for their help with the technical support during this project.

I remain grateful to my family, friends and dear partner for their loving support during this time. Finally, I wish to acknowledge the laboratory support staff at AstraZeneca R&D, Gothenburg for ensuring the continued availability of resources for smooth laboratory operations.

Setu Dambhare

Popular Science Summary

Cell based models that mimic the alveoli for studying inflammation and fibrosis.

Alveoli are the primary site for gaseous exchange. Embedded deep within the lungs, they assume a thin yet robust architecture. Together with the surrounding cells from blood capillaries, alveolar cells form the air-blood barrier. This interface allows respiratory gases to travel between the air-space in lungs and blood in the capillaries.

The constant process of gaseous exchange is made possible by a combined function of many physical and structural components in the alveolar environment. The extracellular matrix and fibroblasts from the alveolar interstitial space, as well as the lining fluid inside the alveoli ensure their stability. Any disruptions to this complex organisation can result in serious dysfunctions as seen in many lung diseases like chronic obstructive pulmonary disorder, idiopathic pulmonary fibrosis and acute respiratory distress syndrome. This necessitates the study of alveoli in health and disease, probing a great need for reliable tools to mimic the alveolar structure and functions outside the human body.

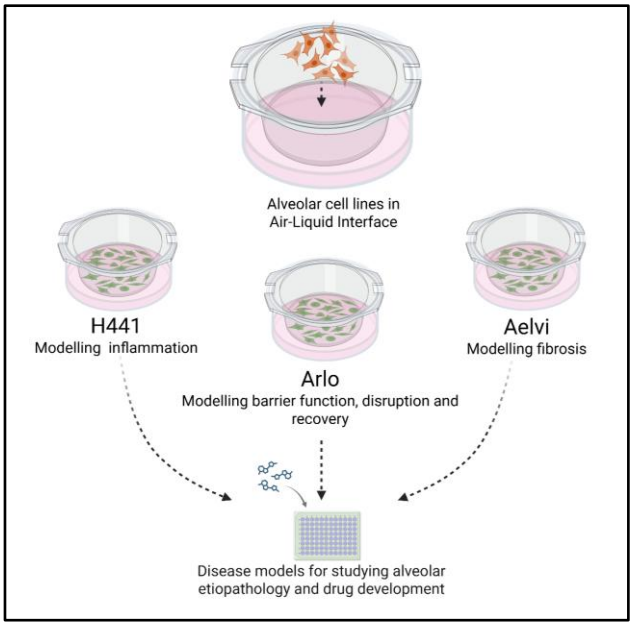

Although the complexity of alveolar architecture is hard to replicate in the lab, this study shows that different cell-lines can demonstrate specific alveolar functions. We grew the cells on top of a permeable membrane and provided media from below the cell layer. The upper portion remained exposed to air, forming an air-liquid interface. This replicated the natural environment to facilitate growth of compact cell layers as seen in the alveoli. Once fully grown, the cell layers formed a strong barrier like the alveoli whose strength could be monitored through measuring the transepithelial electrical resistance.

After comparative evaluation of four cell lines in air-liquid interface, this study characterised three functional systems with different strengths and disease modelling capacity. The cancerous H441 cells formed thick and compact layers. This model showed strong presence of surfactant producing cells in the alveoli and released cytokines as seen in acute phase inflammation related to COPD and Asthma. Immortalised Arlo cells developed a highly responsive barrier suitable for studying structural disruptions in conditions like emphysema where the walls between the alveoli are disrupted. Finally, Aelvi cells, which are the mother cell line of Arlo, formed the strongest barrier and showed strong potential as a tool to study fibrosis.

This study emphasizes the importance of culturing technique in successfully mimicking the alveolar characters. A major strength of this work lies in findings that clarify the suitability of different cell systems in representing different disease conditions. With more characterisations of their genome and proteome, their comparative strengths can be further established. Nevertheless, this work forms the basis for creating flexible models that can be adapted to study different diseases and test therapeutic compounds.

Master's Degree Project in Molecular Biology 60 credits 2025
Department of Biology, Lund University
Advisor: **Jenny Horndahl, Linda Yrlid**
Respiratory and Immunology - COPD-IPF, AstraZeneca R&D